6-1-2006

Numerical modeling of infill RC walls in seismic retrofit of RC frames

Mohamed Darwish

The American University in Cairo
School of Sciences and Engineering
Interdisciplinary Engineering Programs

Numerical Modeling of Infill RC Walls in Seismic Retrofit of RC Frames

by

Mohamed Mohamed Salah El-Din Darwish

A thesis submitted in partial fulfillment of the requirements for the degree of

Master of Science in Engineering

with specialization in:

Construction Engineering

under the supervision of:

Dr. Medhat Haroun
AGIP Professor, Department of Construction Engineering
And Dean, School of Sciences and Engineering
American University in Cairo

Spring 2006

Dedication

To the person who has helped me most in my life, to my mother, I dedicate this thesis.

Acknowledgements

I acknowledge my family for the efforts of the twenty four years of my life.

I acknowledge my honorable professor Dr. Medhat Haroun as he did not only teach me in his field of specialization but he also taught me how to be a researcher and I wish I succeeded to benefit from a landmark as Dr. Haroun.

I acknowledge my colleague Ahmed Mahdy as he provided me with several resources concerning the technical issues in this thesis.

I acknowledge the Interdisciplinary Engineering Program (IEP) for providing the software that was used in this research.

I acknowledge the American University in Cairo for granting me the merit fellowship along my graduate studies.

Abstract

The American University in Cairo

Numerical Modeling of Infill RC Walls in Seismic Retrofit of RC Frames

by
Mohamed Mohamed Salah El-Din Darwish

under the supervision of
AGIP Professor Medhat Haroun
Dean, School of Sciences and Engineering

Spring 2006

Columns designed and built according to older standards may be subject to damage due to seismic loading during earthquakes as a result of the lack of shear reinforcement and/or insufficient lap-splice length. An experimental program on the use of ifill RC walls in seismic retrofit of RC frames under cyclic loading was conducted in 2002. The output of this experimental work formed the basis for the validation of a numerical finite element model, in predicting forces and displacements.

Subsequently the finite element model was used to perform a parametric analysis on the effects of the thickness, overall reinforcement and concrete strength of the infill wall on the seismic strength of the overall system. There was no evidence that the percentage of steel reinforcement in the infill wall had a measurable effect on its seismic behavior. The minimum thickness of the wall to achieve the desired seismic strength of the frame-wall system was determined and illustrated by an empirical formula. The effect of the amount of the steel in the columns on the seismic strength of the system is significant but its effect on the cracking patterns in the wall has been proven to be small. The strength of concrete of the wall had a varying effect on the overall seismic strength of the wall which has also been illustrated in an empirical formula.

The developed finite element model has been proven successful in modeling the major characteristics of the wall-frame system, and therefore, can be applied as a tool for an effective design of such a seismic strengthening system.

Table of contents

List of Figures

List of Tables

CHAPTER 1: INTRODUCTION

1.1 Earthquakes

Earthquakes are ground vibrations caused mainly by the fracture of the earth's crust or by a sudden movement along an already existing fault (tectonic earthquakes). Very rarely, earthquakes may be caused by volcanic eruptions. A widely accepted and well-established theory for the origin of tectonic earthquakes is the 'elastic rebound theory' which was developed in 1906 by Reid [1]. According to this theory, earthquakes are caused by the sudden release of elastic strain energy in the form of kinetic energy along the length of a geological fault. The accumulation of strain energy along the length of geological faults can be explained by the theory of the motion of lithospheric plates into which the crust of the earth is divided. These plates are developed in oceanic rifts and they sink in the continental trench system [1].

The boundaries of the lithospheric plates coincide with the geographical zones which

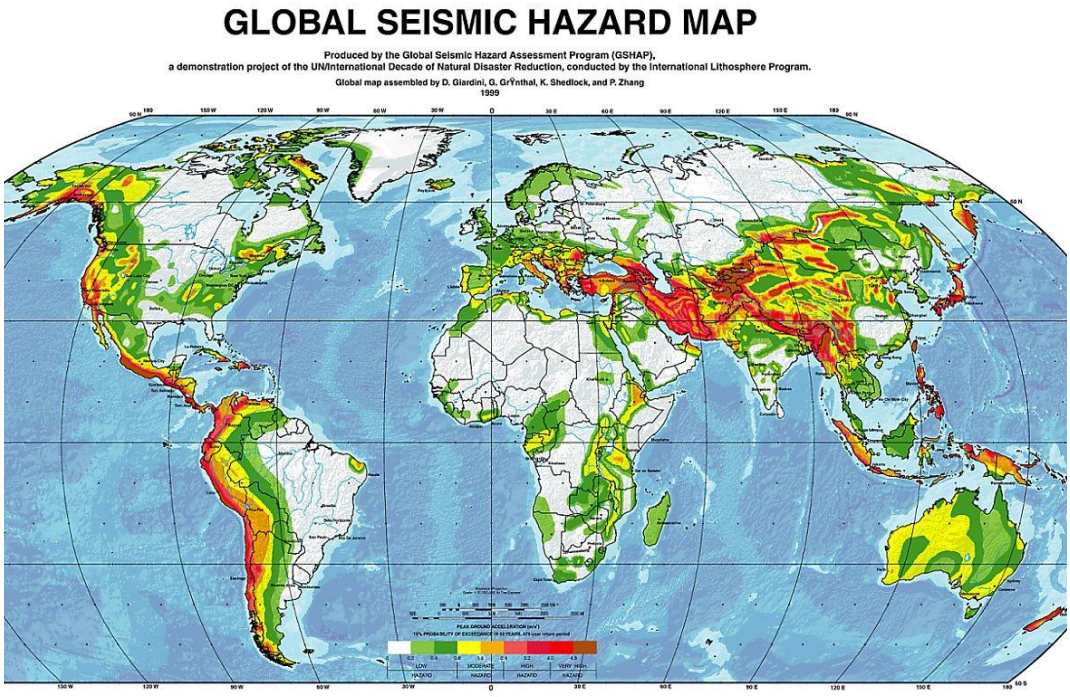

Figure 1.1 A map showing the distribution of earthquakes. [2]

experience frequent earthquakes. The earthquake, considered as the independent natural phenomenon of vibration of the ground, in very few cases poses a threat to humans, as for example when it causes major landslides or tidal waves (tsunamis). An

earthquake becomes a dangerous phenomenon only when it is considered in relation to structures. Of course, the problem is the vibration of the structure under seismic excitation and not the earthquake itself. This is because the structural system is basically designed for gravity loads and not for the horizontal inertia loads that are generated due to ground accelerations during an earthquake. Since the early steps of the technological development of mankind, the joy of creation has been associated with the fear that some superior force would destroy, in a few seconds, what was built with great efforts over a lifetime. In other words, the earthquake problem has always been associated with structure and, therefore, it mainly concerns the structural engineer [1].

Although destructive earthquakes are confined to certain geographical areas known as the seismic zones, the large-scale damage that they may cause in densely populated areas and the associated number of deaths is such that they have an impact on the whole world (Fig. 1.1 & 1.2). Earthquakes, because of the deaths and the damage to buildings that they cause, have several economic, social, psychological and even political effects in the areas and the countries where they take place (Fig. 1.3). Thus, many scientists must deal with this problem, such as seismologists, engineers,

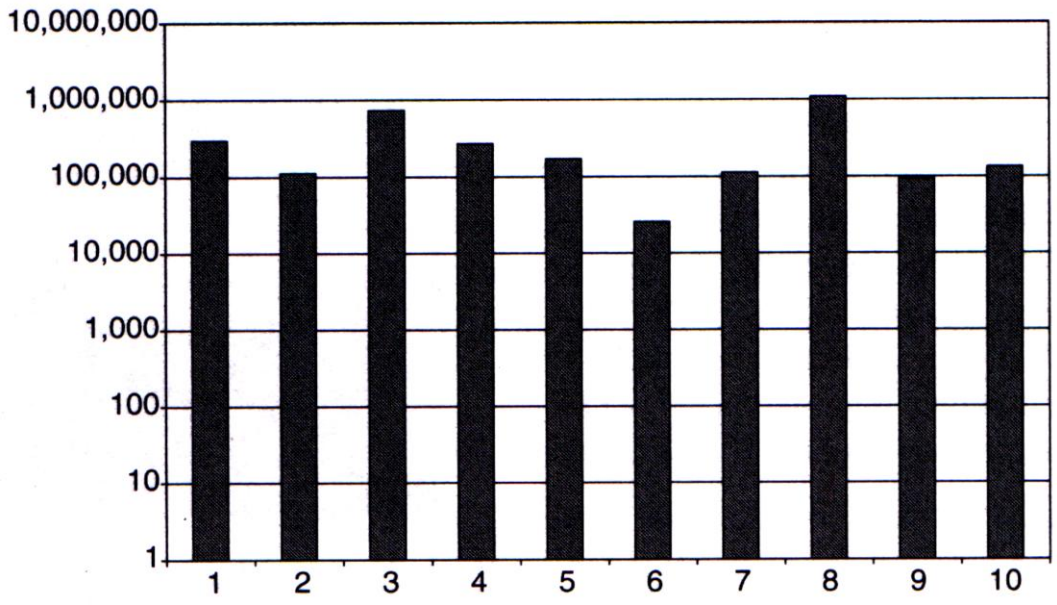

Figure 1.2 Human casualties due to earthquakes in the last ten decades. [2]

psychologists, economists and so on. All these scientific disciplines are coordinated by special bodies on national levels and by special institutes of interdisciplinary character, or, at the university level, by interdepartmental cooperation. The goal of all

these efforts is to develop the earthquake-resistant structure, that is, its improvement from the safety-cost point of view, which are two antagonistic parameters [2].

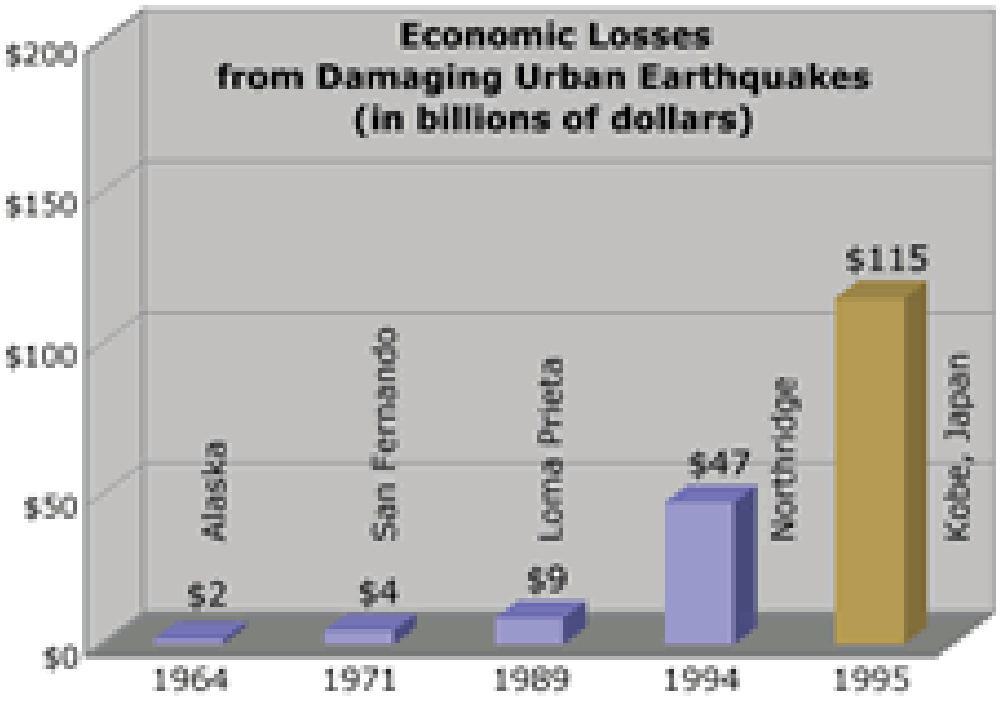

Figure 1.3 The earthquakes causing the largest economic losses in the second half of the 20th century. [2]

1.2 Problem Definition

Columns designed and built according to older standards can be subject to damage due to seismic loading during earthquakes as a result of the lack of shear reinforcement and/or insufficient lap-splice length. Such columns may experience brittle failure modes; hence these columns must be retrofitted so as to adhere to current code requirements and survive future earthquakes.

External jackets have been used frequently so as to increase the ductility of columns. Steel or concrete jackets have been used in many cases to perform that function. However, composite jackets made of fiber-reinforced polymers have gained high credit in the past few years. An alternative retrofit technique that involves the implantation of a reinforced concrete infill wall between the columns of the frame has also been used. The California Department of Transportation (Caltrans) has made use of this system so as to retrofit several deficient column bents in several bridges, especially when the columns are of the rectangular shape (Fig. 1.4) [3].

Figure 1.4 Sample bridge frames strengthened by infill walls in the Los Angeles area. [3]

While the strengthening of an infilled column bent system under lateral static load is well understood, this system was not tested under cyclic or dynamic loading until recently at the University of California at Irvine (UCI) and the University of Nevada at Reno (UNR). In the former structural evaluation program, six one-third scale two-column bents of a typical bridge were tested. The selected bridge model represented the most frequent details and dimensions, and was chosen from among 50 reviewed

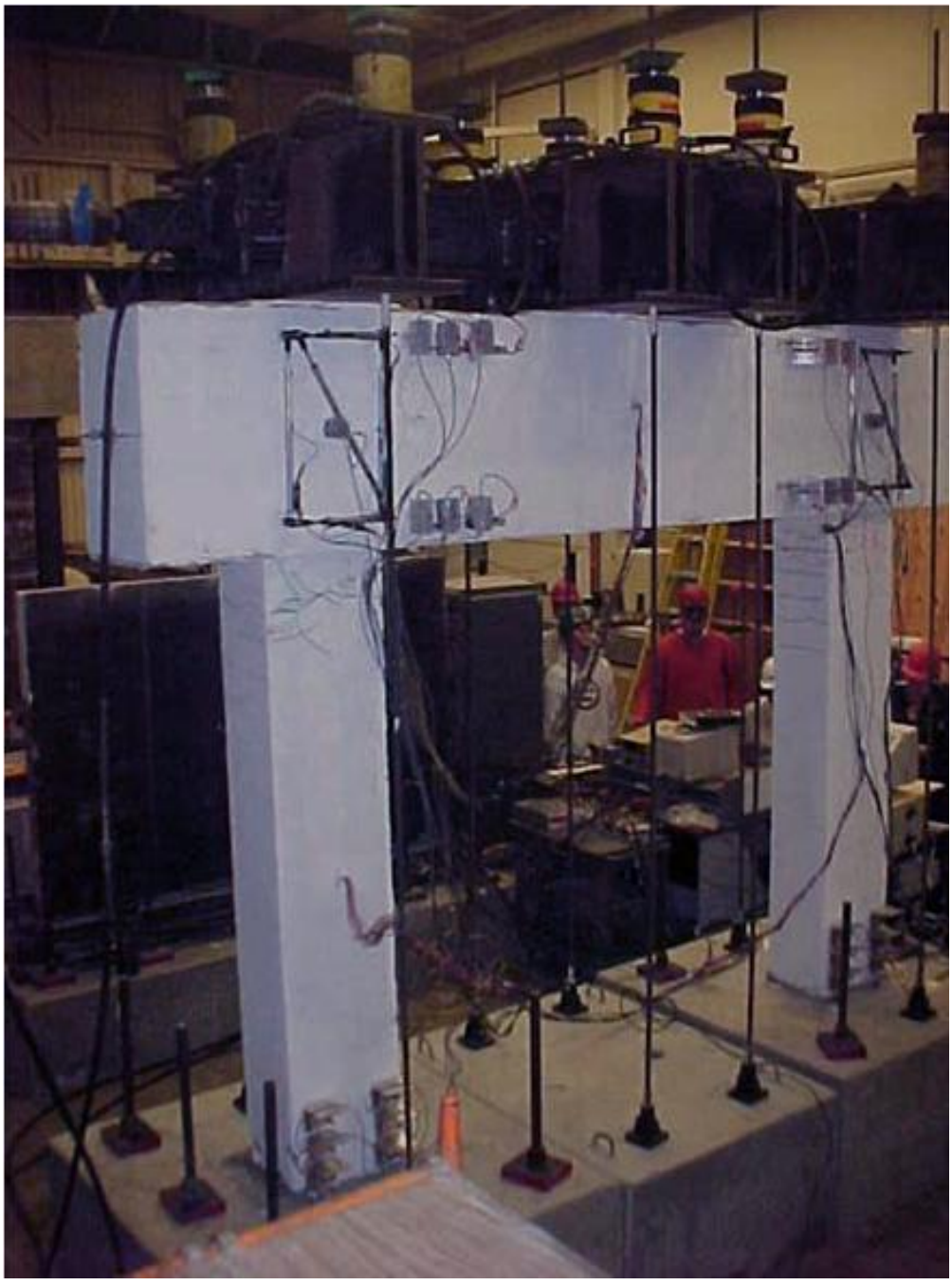

Figure 1.5 Testing of as-built bare column bent. [3]

retrofitted bridges. The six testing samples were: the as-built bare column bent (Fig. 1.5), a column bent sample retrofitted with an infill wall that was anchored to the

columns and the bent cap, a column bent with an infill wall where a gap was left between the wall and the bent cap for field construction purposes (Fig. 1.6), a column bent with an infill wall where the previously mentioned gap was filled with concrete, a column bent with an infill wall where the same gap was allowed and the dowels between the wall and the columns are shorter than the other specimens, and finally, a column bent retrofitted with an infill wall with the gap and the columns were retrofitted with circular concrete jacket at the columns lap splice. Table 1.1 provides a list of all tested column bents and their general configurations [3].

Of course there is a need for a modeling technique to reflect the observed behavior under these tests and for parametric study that measures the sensitivity of the infill wall to changes that could be done to its properties. This parametric study was achieved in this master's thesis using a finite element model on DIANA software.

Figure 1.6 A column bent with an infill wall where a gap was left between the wall and the bent cap for field construction purposes. [3]

Table 1.1 List of all tested column bents and their general configurations [3].

Sample No.	Anchorage to Bent Cap	Embedment Length of Column Dowels	Gap Between Bent Cap and Wall	Lap splice Jacketing
# 1 Bare Column Bent	N/A	N/A	N/A	N/A
# 2 Infilled Column Bent	Yes	Typical	No	No
# 3 Infilled Column Bent with a Gap	No	Typical	Yes	No
# 4 Infilled Column Bent with a Filled Gap	No	Typical	No	No
# 5 Infilled Column Bent with a Gap and Shorter Dowels	No	Short	Yes	No
# 6 Infilled Column Bent with a Gap and Jacketed Lap Splice	No	Typical	Yes	Yes

.

1.3 Objectives of the present study

The present study had a number of objectives summarized as follows:

1. Construct a calibrated numerical model based on the experimental work done by Haroun et al[2].
2. Study the behavior of the infill wall as part of the in-filled frame structural system.
3. Study how the lateral strength is affected by:
    a. The thickness of the infill wall.
    b. The reinforcement of the infill wall.
    c. The concrete strength of the infill wall.
4. Study the effect of the reinforcement of the frame on the cracking pattern of the infill wall.

CHAPTER 2: LITERATURE REVIEW

2.1 Bridges under Seismic Risk

The first United States code specifically addressing highway bridge design was published in 1931 by the American Association of Highway Officials (AASHO), which later changed its name to the American Association of State Highway and Transportation Officials (AASHTO). That code, and subsequent editions prior to 1941, did not address seismic design. The 1941, 1944, and 1949 editions of the AASTHO code mentioned seismic loading, but simply stated that structures should be proportioned for earthquake stresses. Those codes gave no guidance nor criteria as to how the earthquake forces were to be determined or applied to the structure. [4].

Table 2.1 Classification of the seismic risk in U.S. bridges [5].

State	No. of Bridges	States w/PGA $\geq$ 0.1g	States w/PGA $\geq$ 0.2g	States w/PGA $\geq$ 0.3g
California	22261	X	X	X
Connecticut	3749	X		
Dist. Of Columbia	237			
Florida	10188			
Georgia	14226	X		
Hawaii	1043	X	X	X
Idaho	3745	X	X	X
Ilinois	25428	X	X	
Kansas	25648			
Louisiana	14139			
Maine	2583	X		
Michigan	10581			
Minnesota	12994			
Nevada	1073	X	X	X
New Jersey	5997	X		
New York	17326	X		
Oregon	6608	X	X	
Pennsylvania	22457	X		
South Dakota	6822			
Tennessee	18547	X	X	X
Texas	44314			
Virginia	12652	X		
Washington	6898	X	X	X
West Virginia	6513			
Wyoming	2826	X	X	X
Total	298855			

The California Department of Transportation (Caltrans) was the first organization within the United States to develop specific seismic criteria for bridges. This is due to California being one of the states facing the most earthquakes in addition to having a great number of bridges as shown in Tables 2.1 and 2.2 prepared by Saiidi [5]. Caltrans formulated its first general code requirements for bridge design in 1940, and in 1943 included recommendations for specific force levels based on foundation type. In 1965, the Structural Engineers Association of California (SEAOC) adopted provisions where building force levels varied according to the structure type [5].

Table 2.2 The status of the retrofit of bridges in various American states [5].

State	Low seismic area	Selected bridges in review	Evaluate only bridges scheduled for rehab.	Retrofit program being developed or will be soon	Retrofit program has started
California		X		X	X
Connecticut		X			
Dist. Of Columbia			X		
Florida			X		
Georgia	X				
Hawaii				X	
Idaho		X			X
Ilinois		X			X
Kansas					
Louisiana	X				
Maine					
Michigan	X				
Minnesota	X				
Nevada		X			X
New Jersey					X
New York			X	X	
Oregon					X
Pennsylvania					X
South Dakota					
Tennessee			X		
Texas	X				
Virginia				X	
Washington					X
West Virginia	X				
Wyoming		X			

Following the 1971 San Fernando earthquake, which caused several freeway structures to collapse, a bridge-specific code was developed and more stringent seismic force levels were introduced. Most importantly, research was conducted and helped develop a more scientifically based seismic code, including ground motion attenuation, soil effects, and structure dynamic response. Those efforts led to development of the so-called "ARS Spectra," where A, R, and S refer to the maximum expected bedrock acceleration (A), the normalized rock response (R), and the amplification ratio for the soil spectrum (S) [4].

Figure 2.1 A failure in a concrete column in the 1995 Hanshin earthquake in Japan. [2]

According to Chen et al [2] most of the severe earthquake damages to bridges were due to one of three reasons:

1. Unseating of the superstructure at in-span hinges or simple supports due to inadequate seat lengths or restraint. A skewed, curved, or complex configuration further increases the vulnerability.
2. Column brittle failure due to deficiencies in shear design and inadequate ductility. In reinforced concrete columns, the inadequate shear design and

ductility usually stems from inadequate lateral and confinement reinforcement (Fig. 2.1).

3. Unique failures in complex structures e.g. failures occurring in cross-beam or beam-column joints [2].

The second type of failure is the core of this research which makes full use of previous series of research done by several researchers and professors under the supervision and sponsorship of Caltrans.

One of the most frequent techniques was the use of external steel, concrete or FRP jackets to enhance the ductility of bridge columns. An alternative retrofit method that involves the implantation of a reinforced concrete infill wall between the columns of

Figure 2.2 Sample bridge frames strengthened by infill walls in the Los Angeles

the bridge bent has also been implemented. Caltrans has adopted this system to upgrade many under designed column bents, particularly when the columns are rectangular in cross-section (Fig. 2.2) [3].

2.2 Seismic Retrofit Techniques

Seismic strengthening can be achieved using several techniques categorized into three categories [1] (Fig. 2.3):

1. Strength enhancement.
2. Ductility enhancement.
3. Increasing both strength and ductility but at lower values than these achieved in the first two categories.

<u>The strength enhancement techniques can be divided into:</u>

1. Infill walls:
    i. Cast in place reinforced concrete wall (which is the method used in this research).
    ii. Pre-cast concrete wall.
    iii. Ribbed steel panel.
    iv. Concrete or masonry bricks or blocks.
2. Bracing:
    i. Tension and compression cross bracing which could be steel or concrete.
    ii. Tension steel cross bracing.
    iii. K-Braces which could be steel or concrete.
3. Buttressing.
4. Addition of wing walls:
    i. Cast in place reinforced concrete wall.
    ii. Pre-cast concrete wall.

The connection between the infill walls and the frame could be done through dowels which may be anchored, welded or hooked.

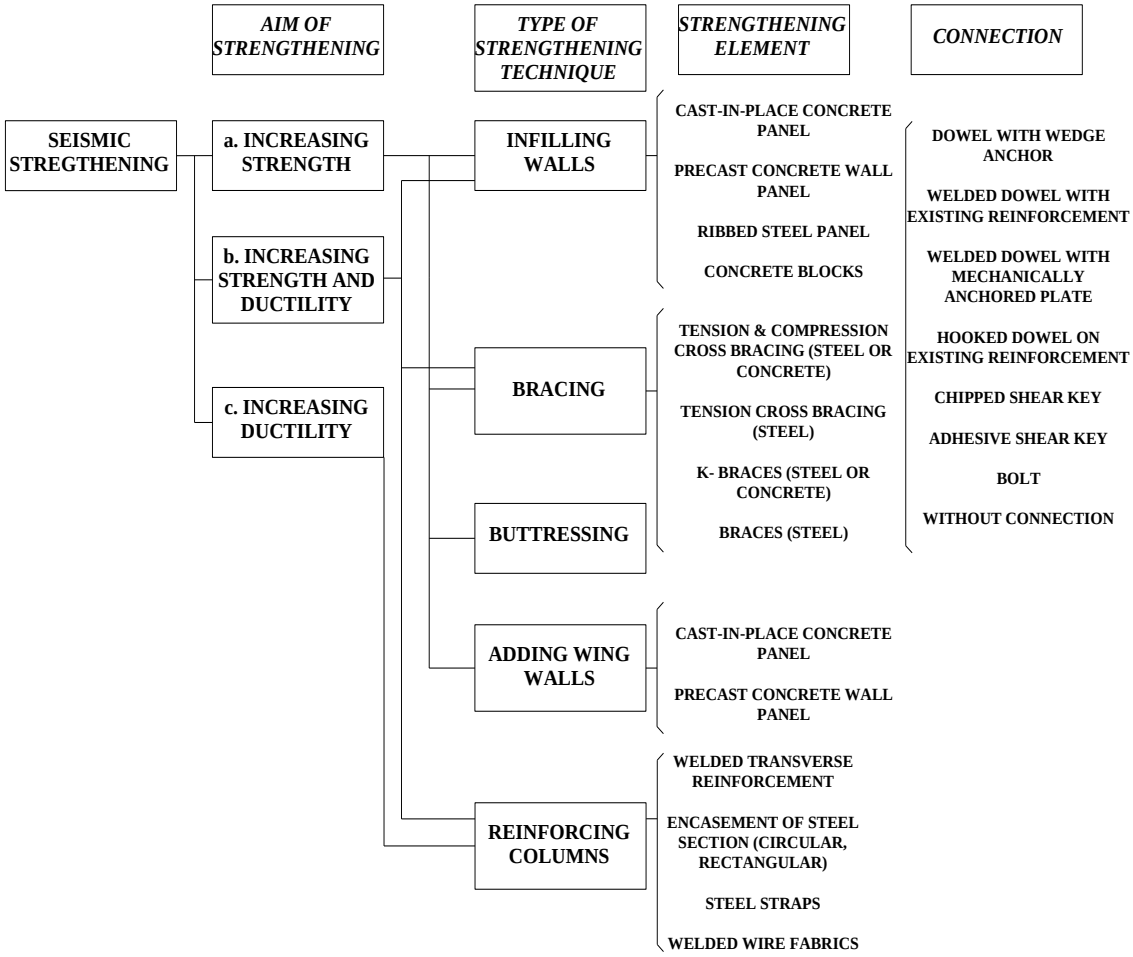

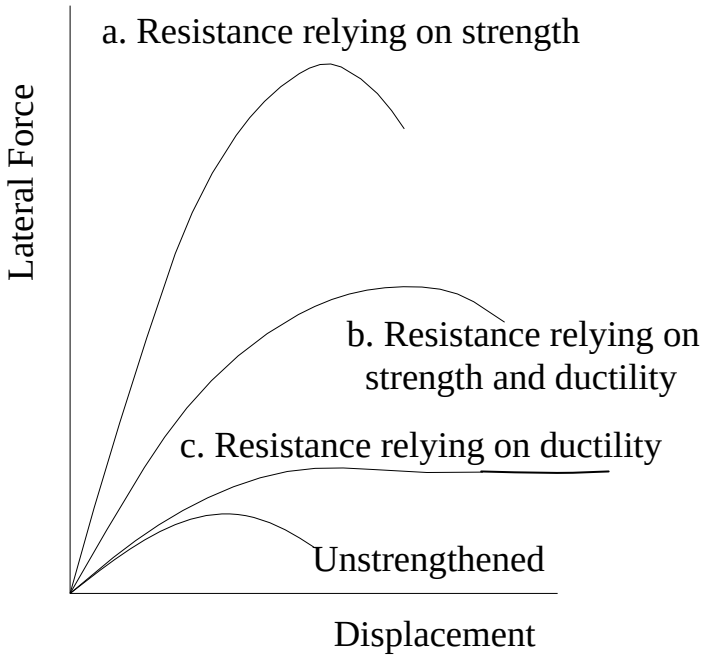

Figure 2.3 Seismic strengthening techniques. [1]

Although several researches were done before on the use of infill walls in seismic strengthening, most of such research was performed using masonry walls. The latest was a paper by Lei et al [6]. This experimental work, done on masonry infill wall, showed that all specimens develop a distinct compression strut mechanism and eventually leads to corner masonry crushing and plastic hinges in the frame members. The infilled masonry significantly improved the initial stiffness and load-resisting capacity of bare RC frames [6].

The fact that the infill wall reduces the sway of the infilled frame was re-assured by Al-Muyeed et al [7]. In this paper, an investigation based on finite element modeling of reinforced concrete frame in the presence of masonry infill subjected to lateral loads was carried out to study the sway behavior of RC frame [7].

The effect of the material properties of masonry infill walls and the size variation effect on the seismic strength of the infill walls have been studied by Hsin et al [8]. This paper presents the results of the experimental and analytical investigations conducted on four 0.8 scale 2-story one-bay ductile reinforced concrete frames with infill nonstructural walls subjected to cyclically increasing loads [8].

In July 2005, Perera [9] published a paper in which a damage model is proposed for the characterization of masonry walls subjected to lateral cyclic loads. The macromodel has been incorporated in a nonlinear structural analysis program for analysis of masonry-infilled RC frames. The model has been validated with some experimental tests. An evaluation of the structural performance of the analysed masonry-infilled frames was performed based on the calculated damage values and the storey drifts [9].

CHAPTER 3: NUMERICAL MODELING

3.1 Introduction

A two dimensional model identical to that tested by Haroun et al [3] was constructed on using a commercial software package "DIANA" that implements the finite element approach. The physical properties, material properties, geometric features, reinforcements, constraints and loads were defined. Subsequently, a nonlinear analysis has been performed. This procedure has been implemented for samples no. 1, 3 and 4 of the test program implemented by Haroun et al [3]. Sample 1 was the control sample, i.e. the bare frame, Sample 3 was the infilled frame with a 2 inch gap left between the bent cap and the wall, while Sample 4 was identical to Sample 3 but the gap was filled with mortar. At last the parametric analysis was performed on Sample 4.

DIANA [10] is a general purpose finite element code, based on the Displacement Method. It has been under development since 1972. One of the most notable aspects in DIANA is its power in the field of concrete and soil where excellent material models are available, developed by researchers in the Netherlands since the early 1970's. Most notably are the models for smeared and discrete cracking, and for reduction of prestress due to special effects. The most important feature in DIANA that was usefull in this research is the special elements used to model embedded reinforcement in concrete structures bars and grids. Various so-called smeared cracking models are available to simulate cracking of brittle materials like concrete. Basically these models are a combination of tension cut-off, tension softening and shear retention criteria. A rate-dependent cracking criterion can be optionally added. The smeared cracking models can also be specified with ambient influence, i.e., dependent of temperature, concentration or maturity. To model these reinforcements DIANA has a built-in preprocessor in which reinforcement can be defined globally. DIANA's strongest points lie in its nonlinear capabilities. For physical nonlinear analysis various material models are available including plasticity, viscoplasticity, cracking, viscoelasticity, creep, hyperelasticity, liquefaction of soil and many more [10].

3.2 Physical properties

In the section of physical properties in DIANA, all the elements used were of the type Q8MEM. This is the four nodded Quadrilateral plane–stress element recommended by DIANA user manual for such a case as all the stresses are in the plane of the frame. Using a plane stress element will save time and space during performing the analysis on the computer. This type of elements is based on linear interpolation and Gauss integration. The thickness of the element in the frame was 12 inch (305 mm), while the thickness of the element in the infill wall was 6 inch (152 mm).

3.3 Material properties

In the section of Material properties in DIANA, using the Elastic aspect and the Isotropic concept a Young's modulus E = 7500000 psi (51.71GPa) and a Poisson's ratio = 0.2. The nonlinear material properties for concrete were defined via the Static Nonlinearity aspect and the "Concrete and brittle materials" then a subset called "Multidirectional fixed crack" was used in which a branch named "Constant stress cut-off" was chosen and another branch from it named "Linear tension softening" then choosing "Ultimate strain based" and "Constant shear retention" and "Vonmises plasticity" was used choosing "Ideal plasticity" concepts filling in the parameters for tensile strength ft = 900 psi (6.21 MPa), ultimate strain ε = 0.003, a constant shear retention factor β = 0.07 and a compressive strength fc = 5000 psi (34.5 MPa).

The values for the compressive and tensile strengths together with the modulus of elasticity have been factored so as to transfer the compressive strength of a concrete cylinder to the compressive strength of a concrete cube, i.e.7000 psi (48.26 MPa). Due to the absence of any experimental value of the shear retention factor, the value of this factor was assumed based on a solved example in the DIANA user manual. This example was recommended by the DIANA online documentation as it includes a frame similar to the frame under study. This value was then adjusted from 0.09 to

0.07 so as to produce a load-deflection curve as near as possible to the experimental load deflection curve [10].

3.4 Constraints

For each of the two columns the node at the lower right corner, the node at the lower left corner together with the node at the midway between them were prevented from motion in the X direction and the Y direction. Therefore each of the two columns is fixed to its footing.

3.5 Incremental Iterative Process

In a nonlinear finite element analysis the relation between a force vector and displacement vector is no longer linear. For several reasons the relation becomes nonlinear, and the displacements often depend on the history of displacements at earlier stages, e.g. in case of plastic material behavior. Just as with a linear analysis, the target is to calculate a displacement vector that equilibrates the internal and external forces. In the linear case, the solution vector could be calculated right away but this is not the case in the nonlinear analysis. To determine the state of equilibrium one not only makes the problems discrete in space (with finite elements) but also in time (with increments). To achieve equilibrium at the end of the increment, one can use an *iterative* solution algorithm. The combination of both is called an *incremental-iterative* solution procedure (Fig. 3.1) [10].

Consider a vector of displacement increments that must yield equilibrium between internal and external forces, and a stiffness matrix relating internal forces to incremental displacements. In reality the physical meaning of items in the displacement vector can also be a velocity or a Lagrange multiplier. In this case the physical meaning of what one calls the displacement and force vector and the stiffness matrix is irrelevant. Most often it represents a continuous system that is approximated using the Principle of Virtual Work, Galerkin discretization or another method [10].

In nonlinear analysis the internal force vector usually depends nonlinearly on the displacements (e.g. nonlinear elasticity). It can also depend on the displacements in

the history. This is the case if the material is `path dependent' such as in plasticity and if large displacements facilitate multiple equilibrium solutions.

To enable a numerical solution, a time discretization is performed. Here `time' can have a real physical meaning e.g. in a creep analysis or it can be a pseudo-time, only to describe a sequence of situations. Starting at time *t* with an approximated solution ${}^{t}\mathbf{u}$, a solution ${}^{t+\Delta t}\mathbf{u}$ is searched for. Within the time-increment, only the displacements at start and end are known. The internal force vector, which may be path dependent, is calculated from the situation at time *t*, the time increment Δt and the displacement increment $\Delta\mathbf{u}$. The external forces only depend on the current geometry. If one considers only one increment, the time increment and the situation at the start of the increment (history) are fixed. The equilibrium equation within the increment then only depends on $\Delta\mathbf{u}$. One can write the nonlinear problem as: find $\Delta\mathbf{u}$ such that

$$\mathbf{u}^{t+\Delta t} = \mathbf{u}^{t} + \Delta\mathbf{u} \qquad \textbf{(3.1)}\ [10].$$

and, with **g** as the *out-of-balance* force vector (the residual forces).

$$\mathbf{g}(\Delta\mathbf{u}) = \mathbf{f}_{ext}(\Delta\mathbf{u}) - \mathbf{f}_{int}(\Delta\mathbf{u}) = 0 \qquad \textbf{(3.2)}\ [10].$$

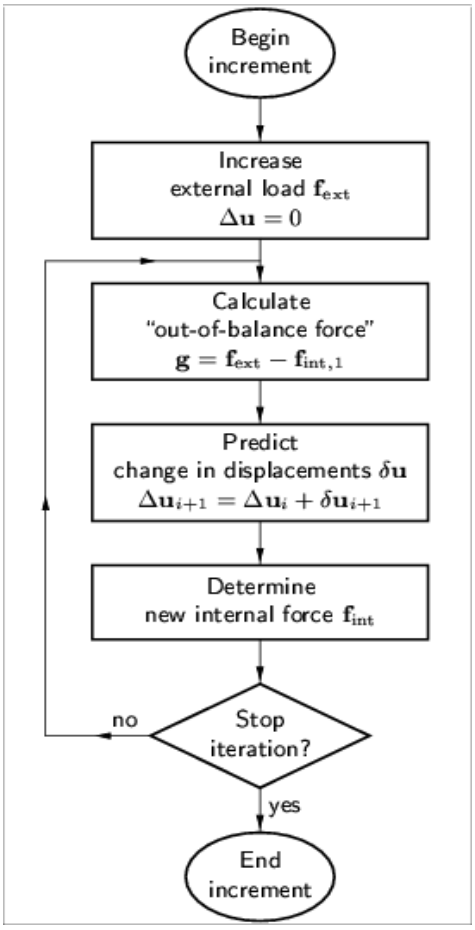

Figure 3.1 The iterative process. [10]

3.6 Newton's Method

The method used by DIANA in this analysis is the Newton's method – also called the Newton-Raphson method. It is a root-finding algorithm that uses the first few terms of the Taylor series of a function f(x) in the vicinity of a suspected root. Newton's method is sometimes also known as Newton's iteration.

The Regular Newton-Raphson method yields a quadratic convergence characteristic, which means that the method converges to the final solution within only a few iterations (Fig. 3.2).

A disadvantage of the method is that the stiffness matrix has to be set up per iteration and, if a direct solver is used to solve the linear set of equations, the time consuming decomposition of the matrix has to be performed per iteration as well. Moreover, the

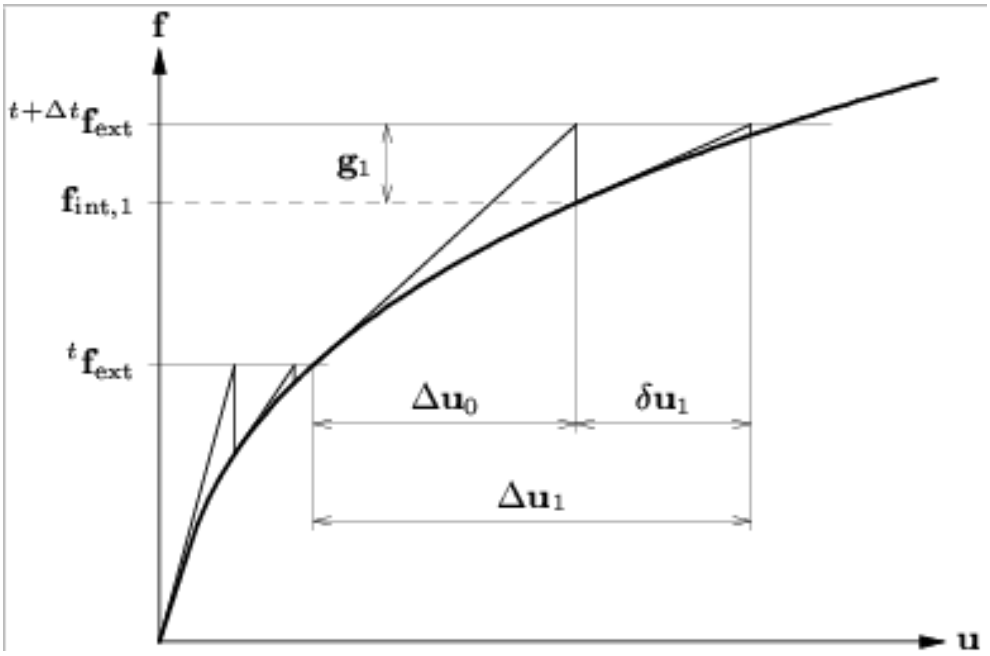

Figure 3.2 Convergence of the regular Newton-Raphson method. [10]

quadratic convergence is only guaranteed if an accurate stiffness matrix is used and if the prediction is already in the neighborhood of the final solution. If the initial prediction is far from the final solution, the method may easily fail because of divergence.

What happened in the models under study was that in many cases the divergence occurred due to the initial prediction falling at an inflection point which needed to increase the maximum allowable number of iterations from 10 iterations to 300 iterations so as to enable the function to be redirected again to a point which is away from this inflection point. [10].

3.7 Convergence Criteria

The iteration process must be stopped if the results are satisfactory (Fig.3.3). For this purpose, DIANA offers several convergence norms. Besides stopping the iteration in case of convergence, the iteration process is also stopped if a specified maximum number of iterations have been reached or if the iteration obviously leads to divergence. The detection of divergence is based on the same norms as the detection of convergence. Figure 3.4 describes the items used to set up the various norms.

The norm used in the models under study was the displacement norm which is the Euclidian norm of the iterative displacement increment. To check convergence, the displacement norm is checked against the norm of the displacement increments in the first prediction of the increment [10].

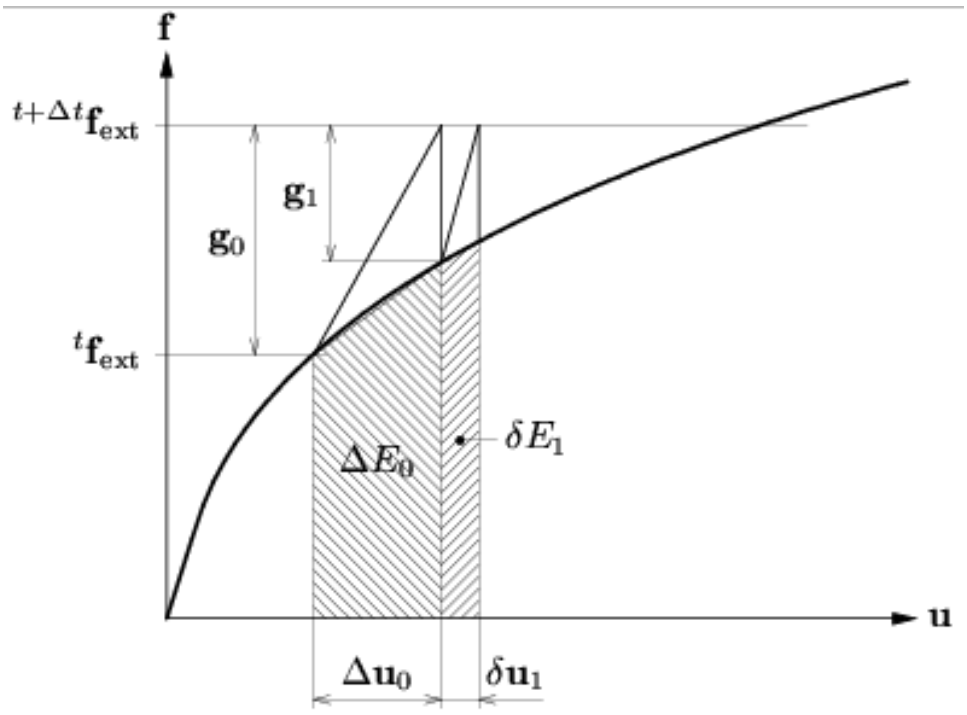

Figure 3.3 The items used to set up the various norms used to test convergence. [10]

3.8 Arc-length Control

In an ordinary iteration process the predictions for the displacement increments can become unrealistic especially if the load-displacement curve is almost horizontal. If a fixed load increment is prescribed, this results in inaccurate predictions for the displacements. The use of an *Arc-length* method overcomes this problem. Using the Arc-length method the *snap-through* behavior can be analyzed, just as displacement control could. Here however it is possible to define a system of loads, which could not be substituted by prescribed displacements. Moreover, the Arc-length method is also capable of passing *snap-back* behavior (Fig. 3.4), where displacement control fails.

The Arc-length method constrains the norm of the incremental displacements to a prescribed value. This is done by simultaneously adapting the size of the increment. Note that the size is adapted within the iteration process and is not fixed at the moment the increment starts. For this purpose we define the external force vector at the start of the increment as ${}^{t}\mathbf{f}_{ext}$ and the increment of the external force vector as $\Delta\lambda_i\underline{\mathbf{f}}$. The load factor $\Delta\lambda_i\underline{\mathbf{f}}$ multiplies a unit load $\underline{\mathbf{f}}$ and can change per iteration. Therefore $\delta\mathbf{u}_i = \mathbf{K}_i^{-1}(\Delta\lambda_i\underline{\mathbf{f}} + {}^{t}\underline{\mathbf{f}}_{int} - \underline{\mathbf{f}}_{int,\,i})$. **(3.2)** [10].

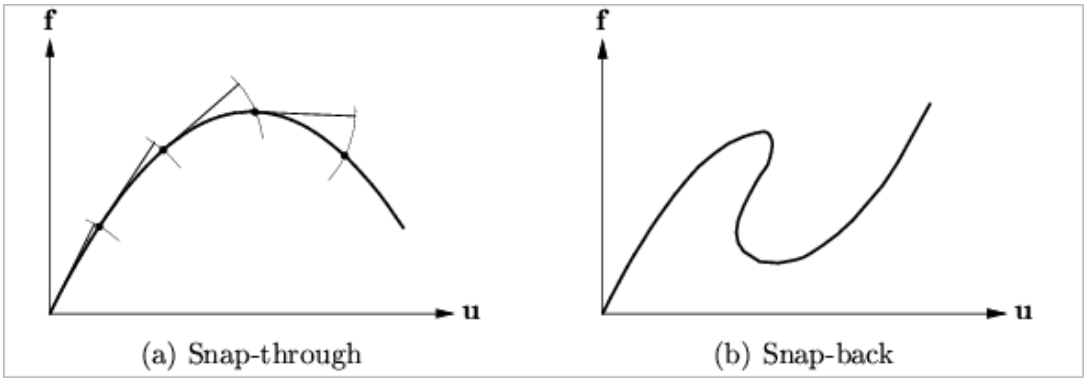

Figure 3.4 Snap – through and snap – back behaviors. [10]

The load factor $\Delta\lambda_i$ is still undefined and can now be used to constrain the incremental displacement vector. DIANA offers a quadratic and a linearized constraint, leading to the *Spherical Path* Arc-length method and the *Updated Normal Plane* method [10].

3.9 Loading steps

The problem understudy is considered to be a special case due to the cyclic load which needs to be represented carefully. According to the DIANA user's manual, attaching a cyclic time curve to the load is the best method. However in the present case, using this method caused divergence when reaching the peak of the time curve (Fig. 3.5).

Hence another method was developed so as to represent the cyclic loading. Cyclic loading was done by applying explicit load steps which are positive until reaching the positive peak then negative until reaching the negative peak. These steps were repeated for three cycles and another three steps with another peak were applied, then several groups of steps with a several peak were applied the failure is reached.

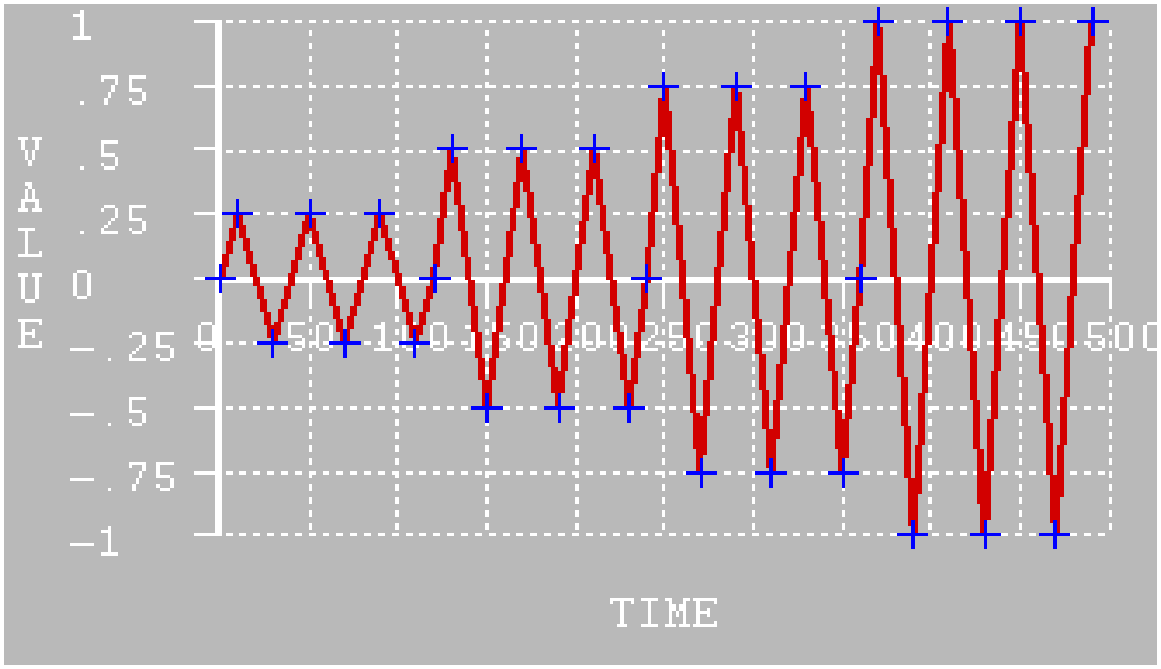

Figure 3.5 Time curve

3.10 Bare Frame

3.10.1 Modeling

The bare frame tested by Haroun et al [3] was analyzed by DIANA software in which the following data were used:

1. Geometric features (Fig. 3.6 and 3.8 and Table 3.1).
2. Material properties (Table 3.1 and section 3.3).

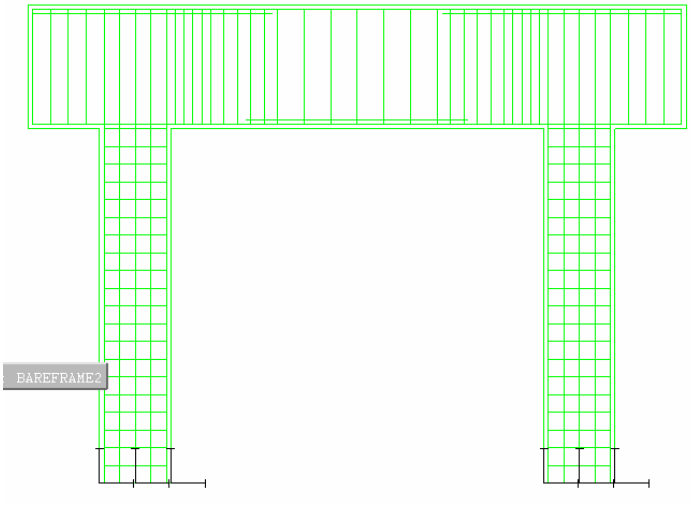

Figure 3.6 R.C. bare frame and its constraints.

3. Physical properties (Table 3.1 and section 3.2).
4. Loads.
5. Constraints (Fig. 3.6 and section 3.4).
6. Meshing (Fig. 3.6).
7. Reinforcements and Lap splice (Fig. 3.8 and Table 3.3).

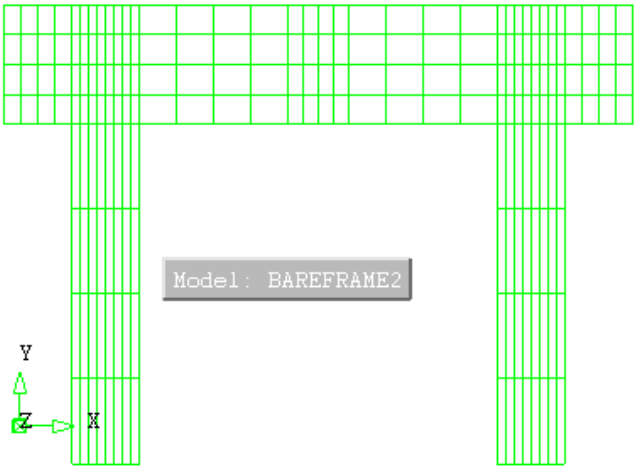

Figure 3.7 Meshing of bare frame.

Table 3.1 Scaling of Columns. [3]

Parameter	Prototype	1/3 Scale
Column dimensions, in (m)	36 x 48 (0.91 x 1.2192)	12 x 16 (0.30 x 0.40)
Height, in (m)	240 (6.10)	80 (2.03)
Bent width, in (m)	240 (6.10)	84 (2.13)
Aspect ratio of bare bent	1	0.95
Cover to longitudinal steel, in (mm)	2 (50.8)	0.7 (17.8)
Concrete strength, psi (MPa)	5000 (45)	5000 (45)
Longitudinal steel area, in^2(cm^2)	25.92 (167.23)	2.88 (18.58)
Longitudinal bar diameter, in (mm)	1.56 (39.6)	0.52 (13.2)
Longitudinal steel	18 # 11	14 # 4
Longitudinal steel ratio	0.016	0.015
Lap splice length, in (mm)	28.2 (716.3)	10 (254)
Transverse steel	# 4	W2 (0.159'')
Spacing of transverse steel, in (mm)	12 (304.8)	4 (101.6)
Core width of column section, in (mm)	32.5 (825.5)	10.8 (274.3)
Core depth of column section, in (mm)	44.5 (1130)	14.8 (375.9)
Volumetric ratio of transverse steel, %	0.149	0.134
Yield stress of column steel, ksi (MPa)	40 (276)	40 (276)

N.B. The values of the concrete compressive strength in MPa have been factored so as to convert them from a cylinder testing system to a cube testing system.

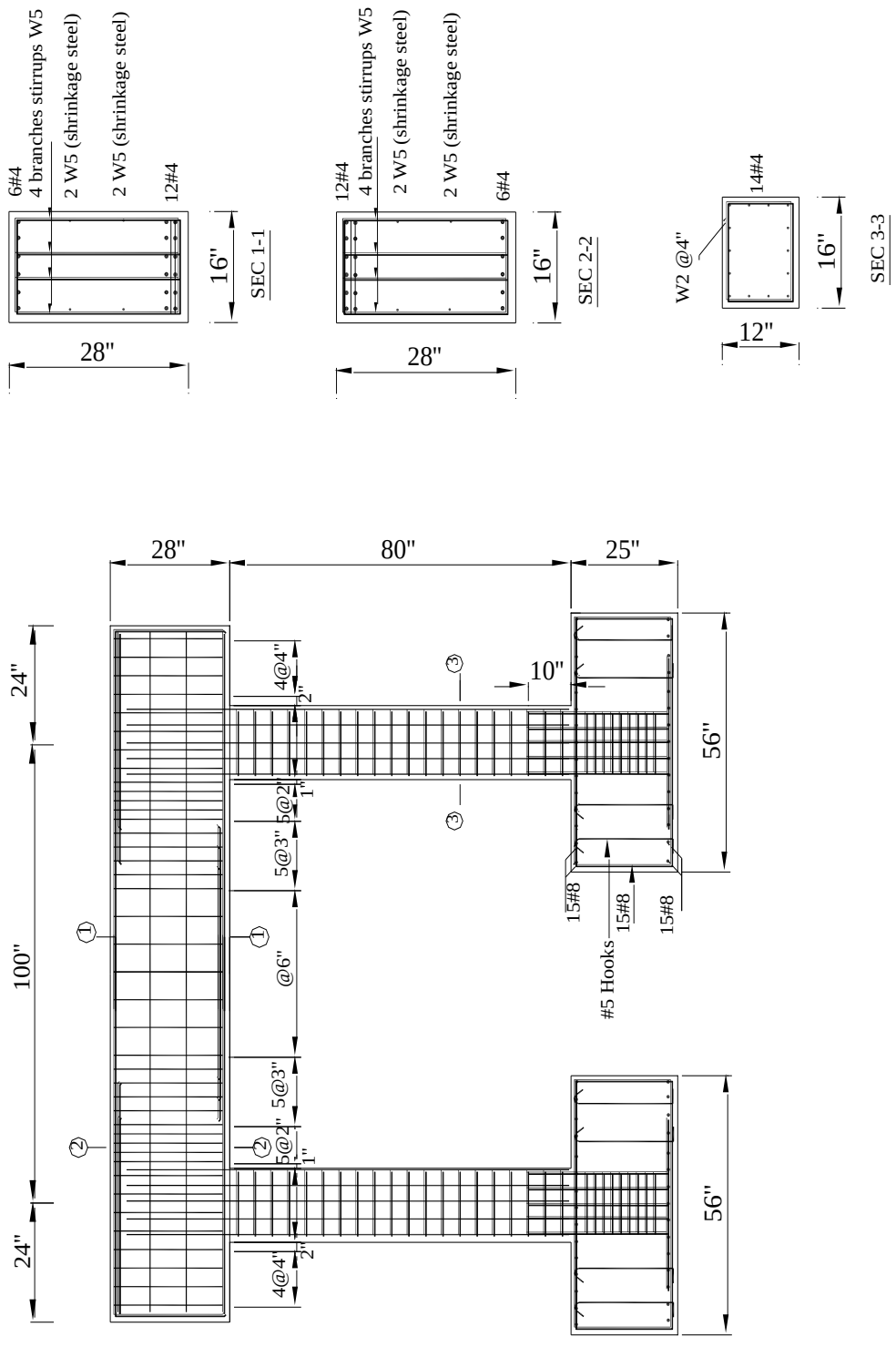

Figure 3.8 Detailing of bare frame. [3]

N.B. 1 inch = 25.4 mm.

3.10.2 Validation under Vertical and Horizontal Static loads

After modeling the bare frame, it was necessary to validate its accuracy by performing a linear analysis and making sure of the following:

1. The deflection under the vertical dead load was symmetric and its shape and intensity was as expected when compared to the output of the same frame when linearly analyzed on SAP. The maximum deflection from DIANA was 0.0857 inch (2.17 mm) while that from SAP under the same load was 0.0751 inch (1.91 mm) which is acceptable due to the fact that DIANA takes the material non linearity and the reinforcement into consideration while SAP does not take these aspects into consideration in addition to the fact that the SAP model was done using one dimensional elements while the DIANA model was done using two dimensional elements. (Fig. 3.9 and Appendix A).

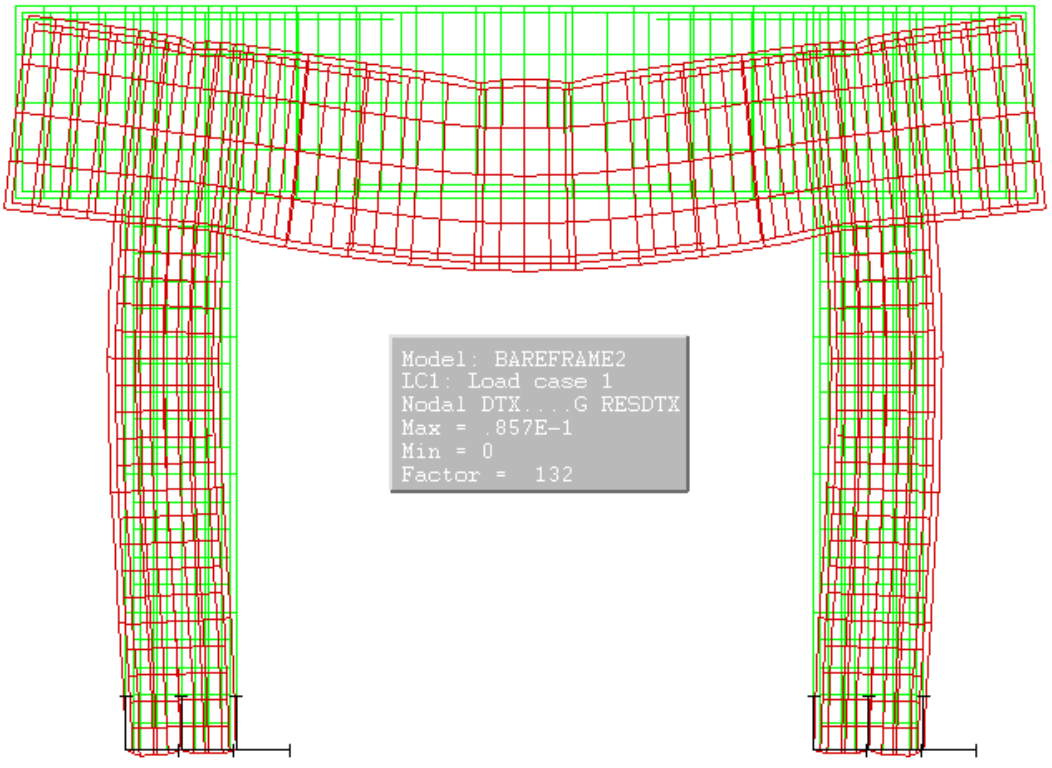

Figure 3.9 Deflected bare frame under vertical dead load.

2. The deflection under the horizontal load looks as expected when compared to the output of the same frame when linearly analyzed on SAP. All the nodes at the same level have the same deflection in the horizontal direction. The Deflection from DIANA was 0.458 inch while that from SAP under the same load was 0.518

inch which is acceptable due to the fact that DIANA takes the material non linearity and the reinforcement into consideration while SAP does not take these aspects into consideration in addition to the fact that the SAP model was done using one dimensional elements while the DIANA model was done using two dimensional elements. (Figure 3.10 and Appendix A).

Figure 3.10 Deflected bare frame under the horizontal load.

3. The crack pattern under the horizontal load is as expected in terms of the positions and the shapes of the cracks as the cracks are concentrated at the corners of the frame (Fig. 3.11).

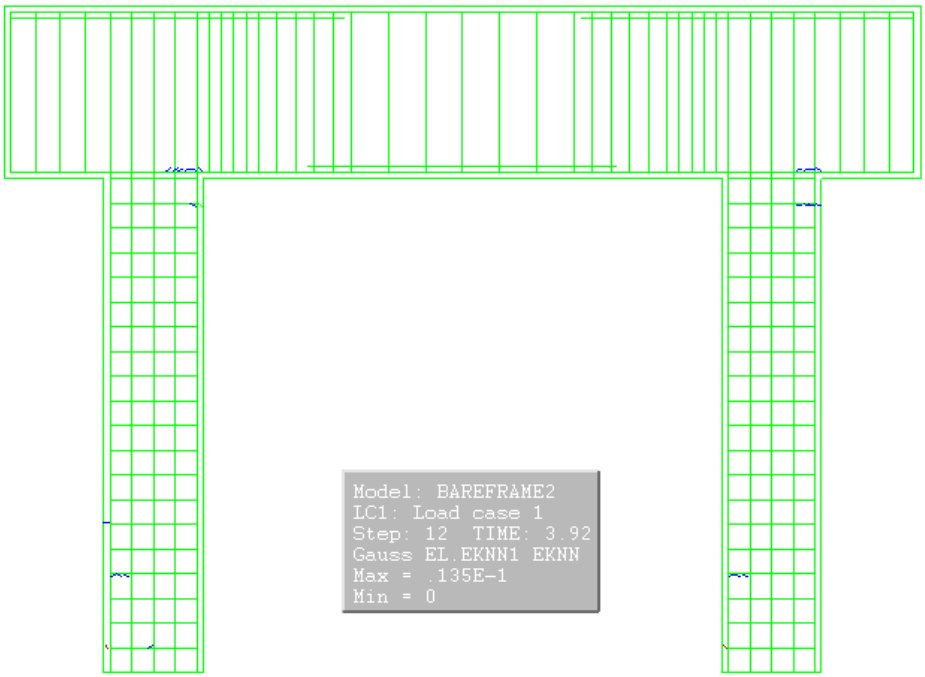

Figure 3.11 Cracked bare frame under the horizontal load.

3.10.3 Calibration of the Cyclic Performance

So as to perform an acceptable analysis in terms of accuracy the bare frame must be calibrated in terms of the model used to represent the material properties as accurate as possible (section 3.3) and the loading conditions (See the Command file in Appendix B). A nonlinear analysis was performed on the bare frame so as to reach results which are acceptable when compared to the original experimental results. To achieve this, the loading process was done as similar as possible to the experimental (See the Command file in Appendix B):

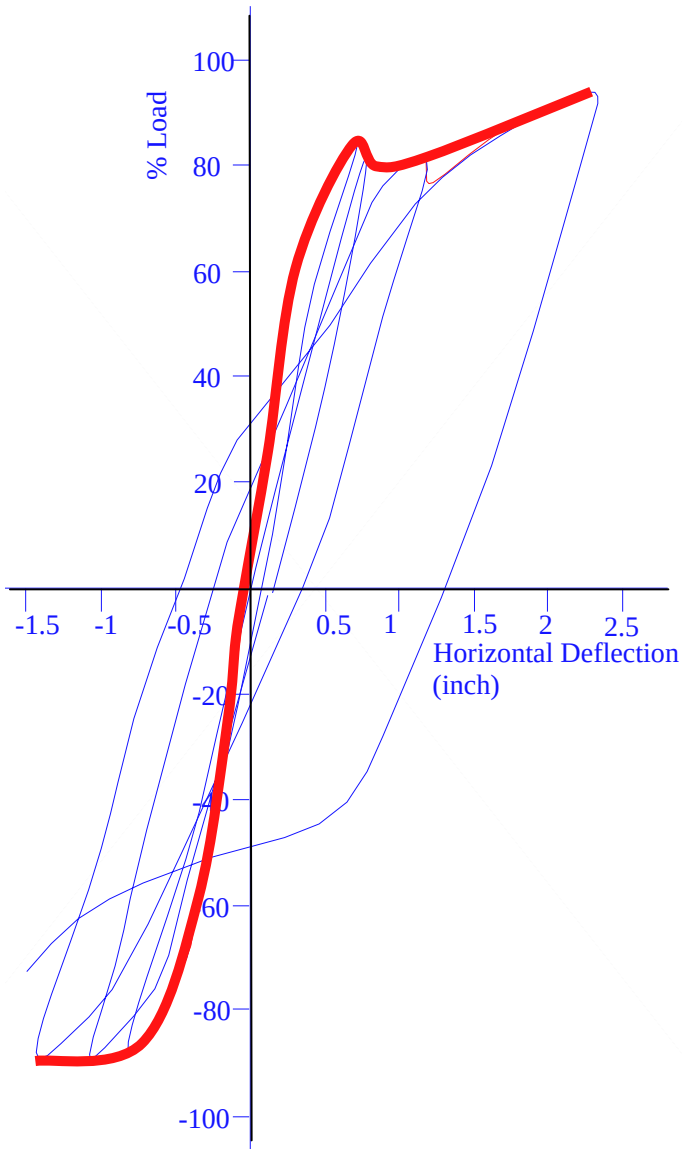

Figure 3.12 Cyclic load – deflection curve for bare frame

1. Three cycles with an amplitude of 16.7 Kips (74.3 KN) which is equivalent to 25% of the seismic load.
2. Three cycles with an amplitude of 33.4 Kips (148.6 KN) which is equivalent to 50% of the seismic load.
3. Three cycles with an amplitude of 50.1 Kips (222.9 KN) which is equivalent to 75% of the seismic load.
4. Three cycles with an amplitude of 54.78 Kips (243.7 KN) which is equivalent to 82% of the seismic load.
5. Apply the full seismic load until failure.

The result of the calibration process was the frame failing at a load of 63.126 Kips (297.1 KN) which is 94.5% of the experimental seismic load having a maximum deflection of 2.3 inch (58.4 mm) which was 2.1 inch (53.3 mm) in the experiment. (Fig. 3.12 and 3.22 and Table 6). From the Cyclic load – deflection curve shown in Fig. 3.12 it could be said that this curve is symmetric about the origin until reaching the plastic zone then the symmetry is lost due to the presence of residual stresses.

3.11 Infilled Frame

3.11.1 Modeling

The frame infilled with a concrete wall tested by Haroun et al [3] was fed into DIANA software. A full and continuous connection between the frame and the wall was assumed. The following data were inserted:

1. Geometric features (Fig. 3.13 and 3.15 and Table 3.2).
2. Material properties (Table 3.2 and section 3.3).
3. Physical properties (Table 3.2 and section 3.2).

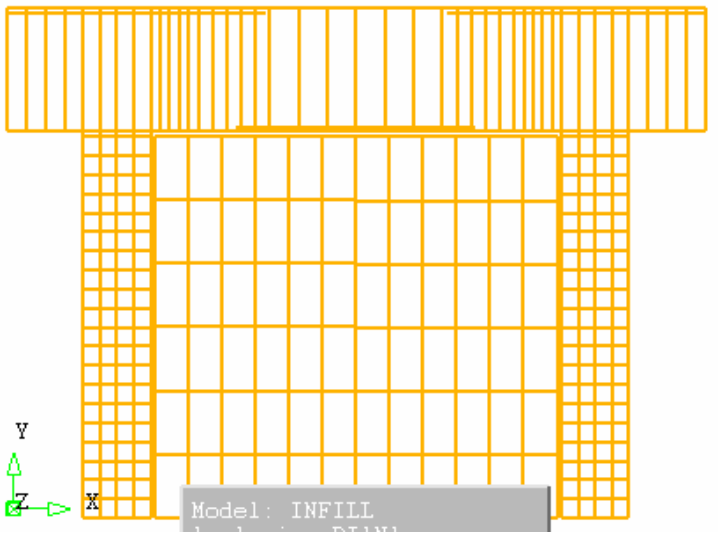

Figure 3.13 R.C. infilled frame.

4. Loads.
5. Constraints. (section 3.4)
6. Meshing (See Fig. 3.14).
7. Reinforcements (See Fig. 3.14 and 3.15 and Table 3.2).

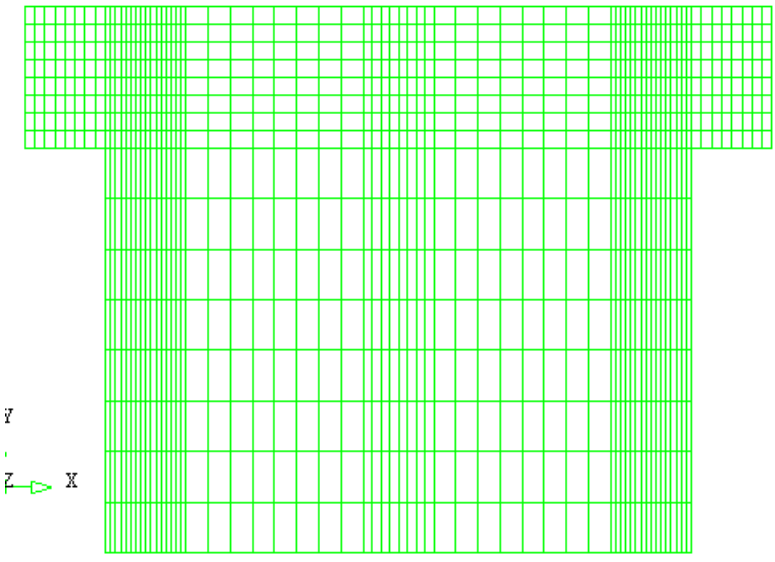

Figure 3.14 Meshing of infilled frame.

Table 3.2 Scaling of infill walls. [3]

Parameter	Prototype	1/3 Scale
Wall thickness, in (mm)	18 (457)	6 (152)
Wall vertical & horizontal steel	# 6	# 2
Spacing between horizontal & vertical steel, in (mm)	12 (305)	4 (101.6)
Cover to horizontal steel, in (mm)	1.5 (38.1)	0.5 (12.7)
Steel ratio, %	0.407	0.417
Crossties	# 5	W3.5 (D = 0.211'')
Spacing between crossties, in (mm)	12 (305)	4 (101.6)
Dowels	# 6	# 2
Spacing between dowels, in (mm)	12 (305)	4 (101.6)
Length of dowels, in (mm)	24 (610)	8 (203)
Hole length, in (mm)	12 (305)	4 (101.6)
Concrete strength, psi (MPa)	5000 (45)	5000 (45)
Yield stress for wall steel, ksi (MPa)	60 (414)	60 (414)
Vertical gap at top, in (mm)	6 (152.4)	2 (50.8)

N.B. The values of the concrete compressive strength in MPa have been factored so as to convert them from a cylinder testing system to a cube testing system.

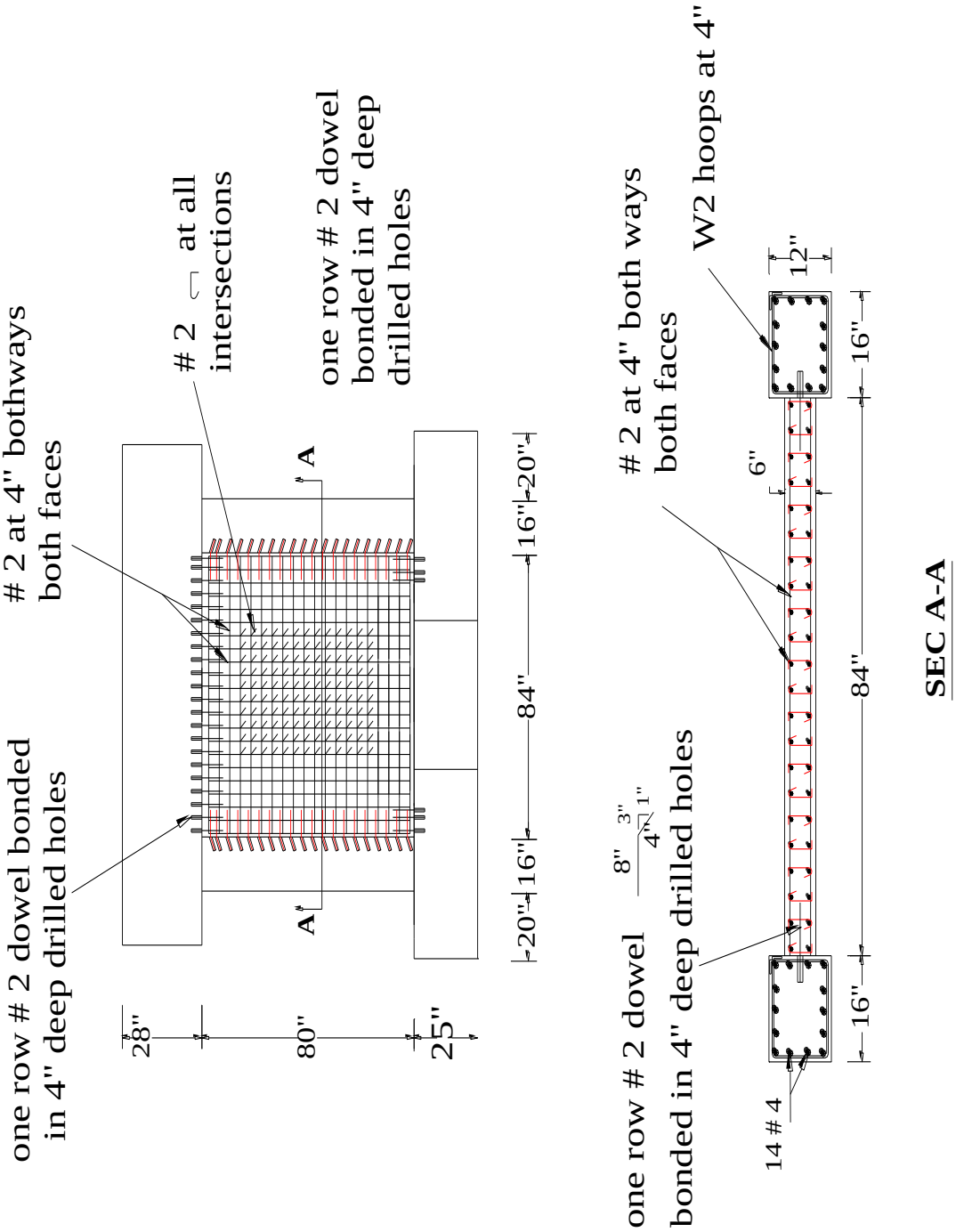

Figure 3.15 Detailing of infilled frame. [3]

N.B. 1 inch = 25.4 mm.

3.11.2 Validation under Vertical and Horizontal Static loads

After modeling the in filled frame it was necessary to validate it i.e. making sure that the general behavior of the modeled structure is as expected which was assured by performing linear analysis and making sure of the following:

1. The deflection under the vertical dead load alone is relatively small when compared to that of the bare frame.
2. The deflection under the horizontal load looks as expected as all the nodes at the same level have the same deflection in the horizontal direction and the highest deflection is at the top of the frame and the deflection of the lowermost nodes is zero. (Fig. 3.16).

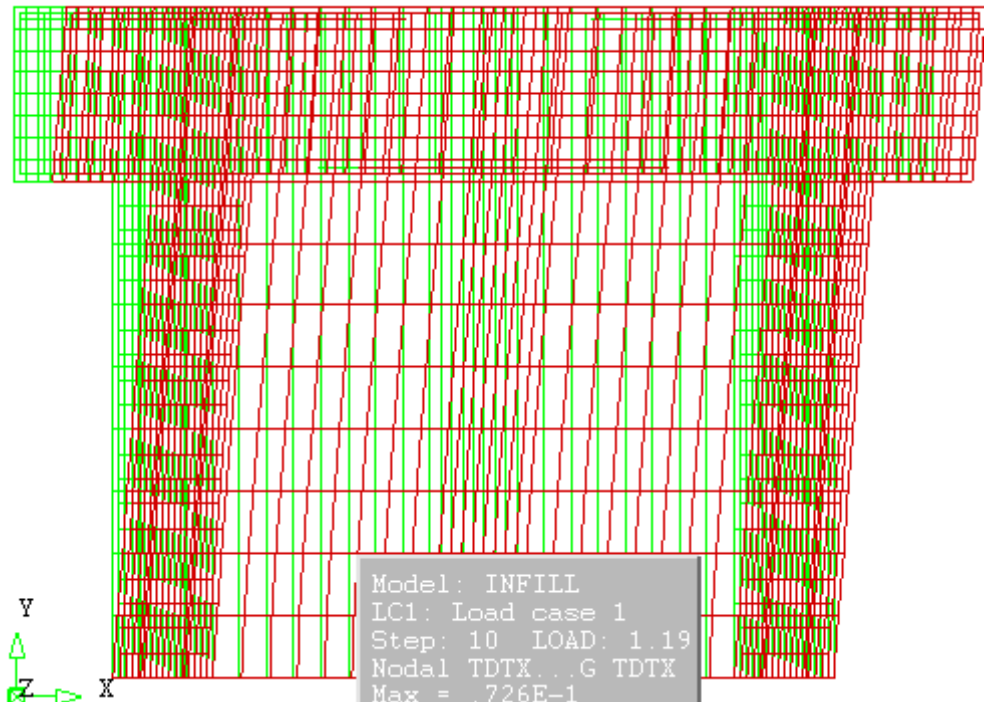

Figure 3.16 Deflection of infilled frame under the horizontal load.

3.11.3 Calibration of the Cyclic Performance

So as to perform an acceptable analysis in terms of accuracy the infilled frame must be calibrated in terms of the model used to represent the material properties as accurate as possible (section 3.3) and the loading conditions (See the Command file in Appendix B). A nonlinear analysis was performed so as to reach results which are acceptable when compared to the original experimental results. To achieve this, the loading process was done as similar as possible to the experimental (See the Command file in Appendix B):

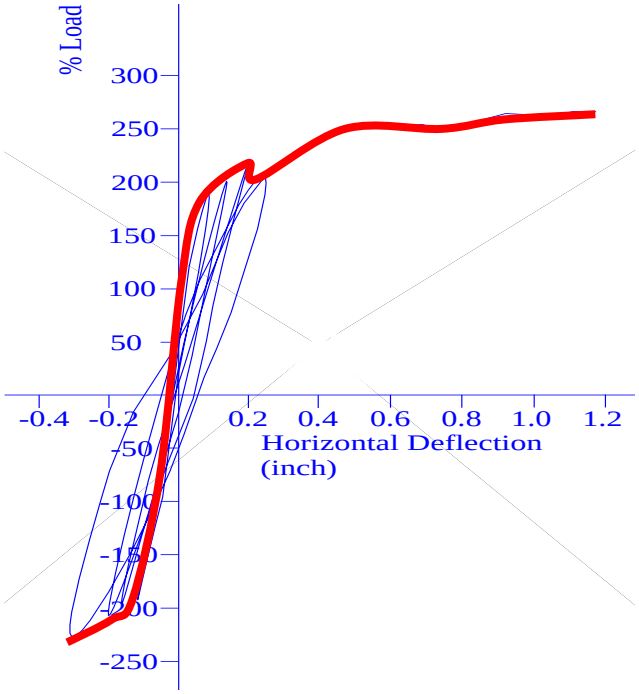

Figure 3.17 Cyclic load deflection curve for infilled frame.

1. Three cycles with an amplitude of 80.16 Kips (356.6 KN) which is equivalent to 120% of the seismic load.
2. Three cycles with an amplitude of 120.24 Kips (534.9 KN) which is equivalent to 180% of the seismic load.
3. Three cycles with an amplitude of 146.96 Kips (653.7 KN) which is equivalent to 220% of the seismic load.
4. Apply 200.4 Kips (891.4 KN) which is equivalent to 300% of the seismic load until failure.

The result of the calibration process was the frame failing at a load of 178.36Kips (793.4 KN) which is equivalent to 267% of the seismic load where as the failure in the experiment occurred at 178 Kips (791.8 KN) which is equivalent to 266% of the seismic load having a maximum deflection of 1.18 inch (29.97 mm) which was 1.05 inch (26.67 mm) in the experiment. (Fig. 3.17 and 3.22 and Table 3.3). From the Cyclic load – deflection curve shown in Fig. 3.17 it could be said that this curve is symmetric about the origin until reaching the plastic zone then the symmetry is lost due to the presence of the residual stresses.

3.12 Infilled Frame with a Gap between the bent cap and the wall

3.12.1 Modeling

The frame infilled with a concrete wall – identical to the frame and the wall mentioned in section 3.11 – was tested by Haroun et al [3] is inputted to DIANA software. In this case a 2 inch gap was left between the frame and the wall. The following data were inputted:

1. Geometric features (Fig. 3.18 and 3.16 and Table3.2).
2. Material properties (Table 3.2 and section 3.3).

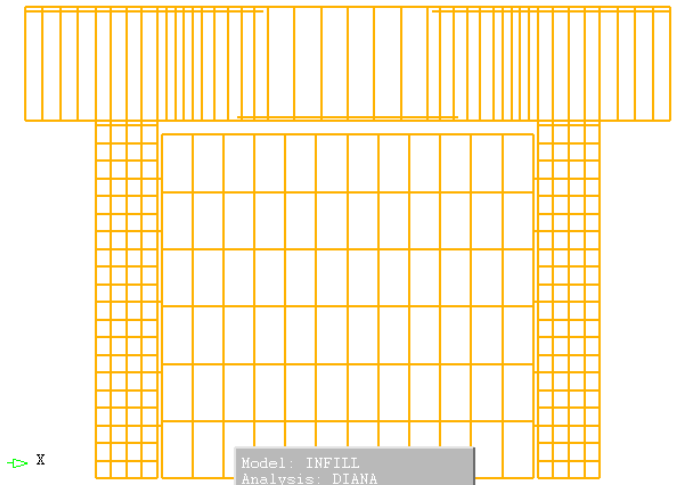

Figure 3.18 R.C. infilled frame with a 2” gap.

3. Physical properties (Table 3.2 and section 3.2).
4. Loads.
5. Constraints. (section 3.4)
6. Meshing: where the new mesh was irregularly divided so as to keep the left side and the right side of the wall in full contact with the columns (Fig. 3.19).
7. Reinforcements (Fig. 3.18 and 3.15 and Table3.2)..

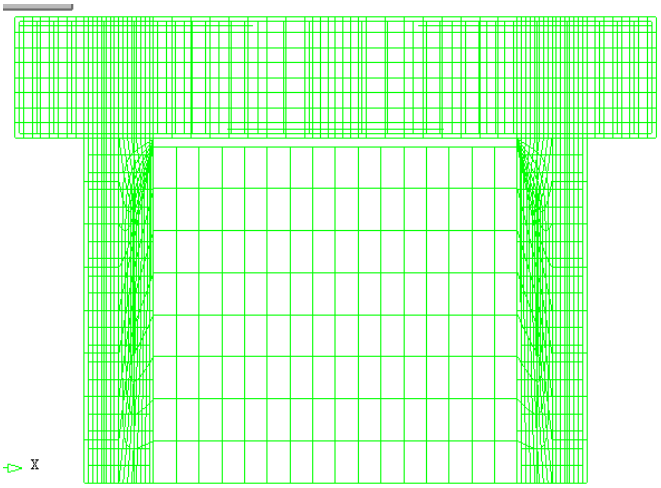

Figure 3.19 Meshing of infilled frame with a 2” gap.

3.12.2 Validation under Vertical and Horizontal Static loads

After modeling the infilled frame it was necessary to validate it i.e. make sure that the general behavior of the structure is as expected which was assured by performing linear analysis and making sure of the following:

1. The deflection under the horizontal load looks as expected as all the nodes at the same level have the same deflection in the horizontal direction and the highest deflection is at the top of the frame and the deflection of the lowermost nodes is zero.
2. The crack pattern under the cyclic horizontal load is as expected in terms of the positions of the cracks and the lengths of the cracks as the longest cracks are emerging from the upper inner corners of the frame and bridging together to make one crack in each column with an angle (Fig. 3.20) while in the experiment the cracks were initiated at the gap but extended excessively in the bent cap.

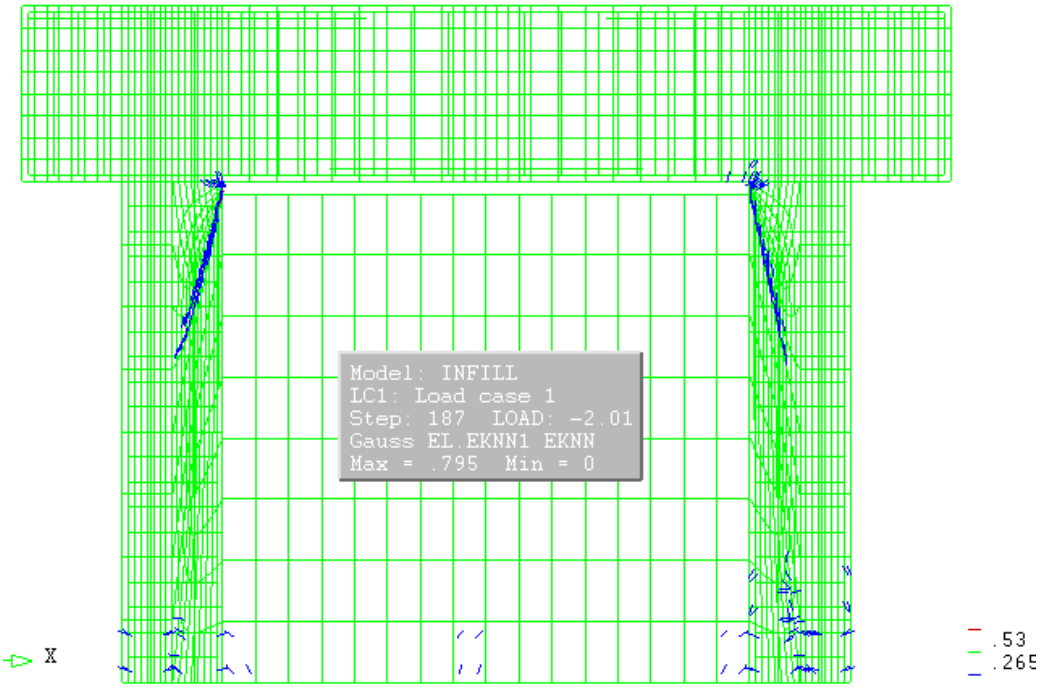

Figure 3.20 Cracks in infilled frame with 2 inch gap.

3.12.3 Calibration of the Cyclic Performance

So as to perform an acceptable analysis in terms of accuracy the infilled frame must be calibrated in terms of the model used to represent the material properties as accurate as possible (section 3.3) and the loading conditions (See the Command file in Appendix B). A nonlinear analysis was performed so as to reach results which are acceptable when compared to the original experimental results. To achieve this, the loading process was done as similar as possible to the experimental loads follows (See the Command file in Appendix B):

1. Three cycles with an amplitude of 80.16 Kips which is equivalent to 120% of the seismic load.
2. Apply 146.96 Kips which is equivalent to 220% of the seismic load until failure.

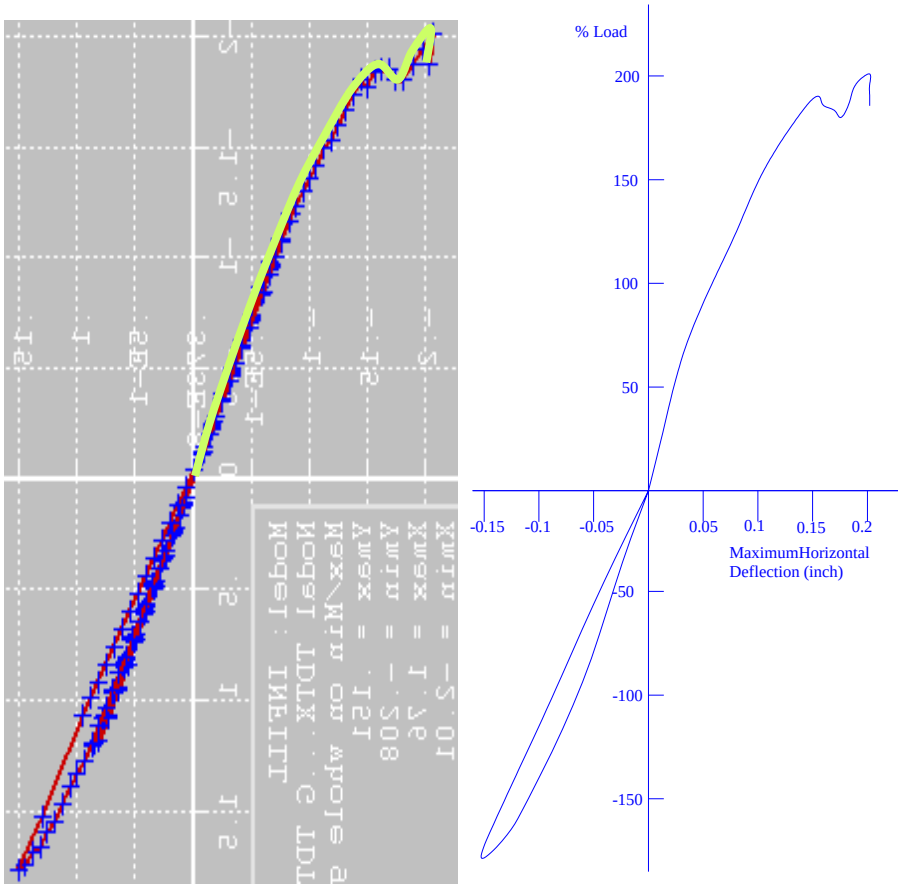

Figure 3.21 The cyclic load deflection curve for infilled frame with a 2" gap.

The result of the calibration process was the frame failing at a load of 134.27 Kips (597.25 KN) which is equivalent to 201% of the seismic load where as the failure in

the experiment occurred at a load of 136.5 Kips (607.18 KN) which is equivalent to 204.3% of the seismic load having a maximum deflection of 0.208 inch (5.28 mm) (Fig. 3.21 and 3.22 and Table 3.3). When comparing the cyclic load–deflection curves shown in Fig. 3.22 it could be said that the sample having the 2” gap was approaching a similar behavior to that with the filled gap but failure occurred earlier.

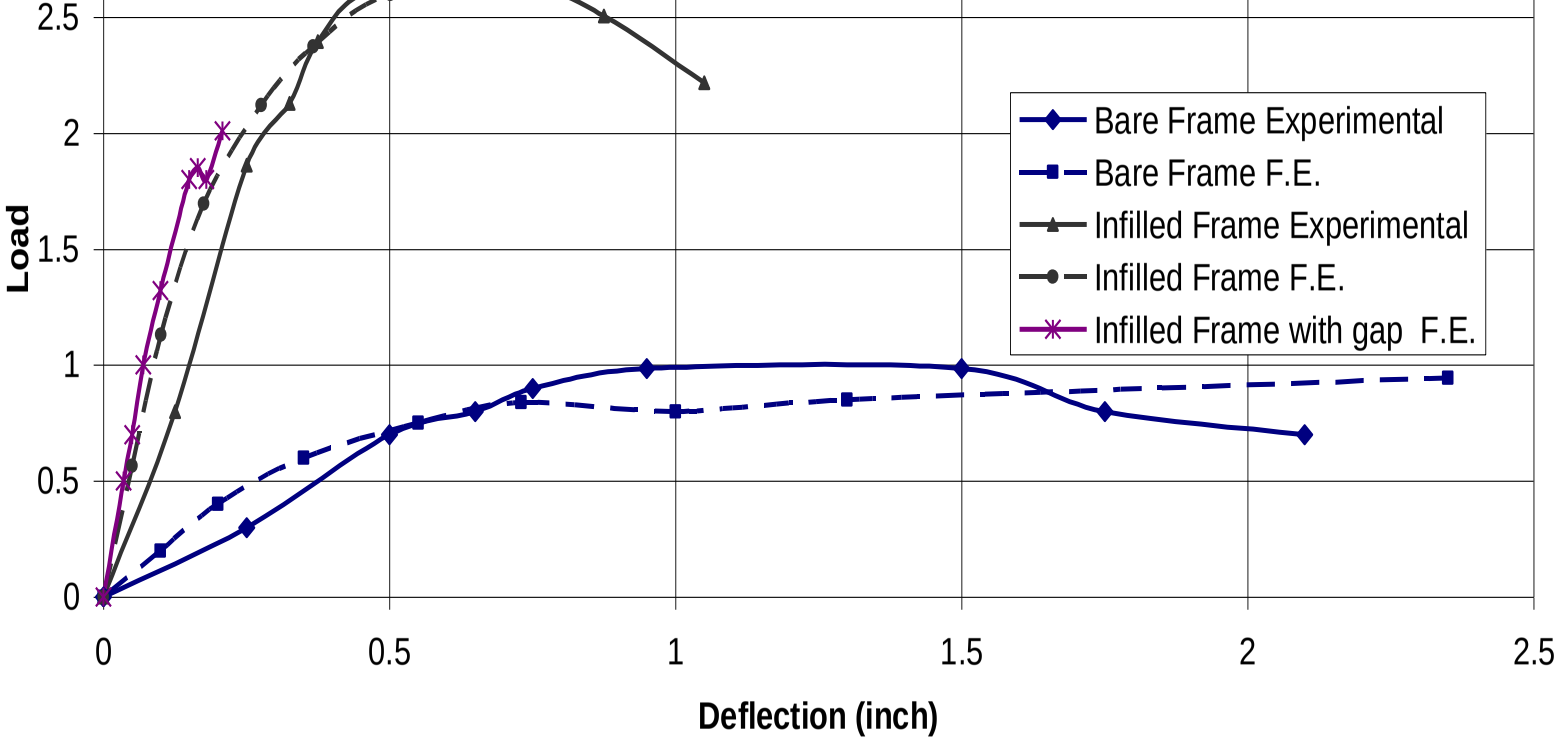

Figure 3.22 Load – Deflection curves for experimental and finite element models.

Table 3.3 Comparison between experimental results and finite element results

Sample No.	*Experimental Results*				*F.E. Results*					
	Maximum lateral load (kips)	Maximum lateral load (KN)	Maximum lateral deflection (in)	Maximum lateral deflection (mm)	Maximum lateral load (kips)	Maximum lateral load (KN)	% Error in Maximum Seismic Force	Maximum lateral deflection (inch)	Maximum lateral deflection (mm)	% Error in Maximum Lateral deflection
# 1 Bare Column Bent	66.8	297.14	2.1	53.34	63.126	280.80	-5.50%	2.3	58.42	9.52%
# 3 Infilled Column Bent with a Gap	136.5	607.18	0.2	5.08	134.27	597.25	-1.64%	0.208	5.283	4.00%
# 4 Infilled Column Bent with a Filled Gap	178	791.78	1.05	26.67	178.36	793.37	0.20%	1.18	29.97	12.38%

The results summarized in Table 3.3 proved that the numerical model of sample # 4 – which was the model used later to perform the parametric study – was highly accurate in representing the maximum lateral strength and 87.6 % accurate in representing the maximum lateral deflection. The numerical model was more accurate in representing the maximum lateral strength than in representing the maximum lateral deflection because the number of cycles applied in the numerical model until failure was not exactly the same as the number of cycles applied until failure in the experiment due to DIANA reducing the step size after each new iteration.

CHAPTER 4 PARAMETRIC ANALYSIS

In this chapter the calibrated model of sample 4 was used to perform a parametric analysis.

4.1 Changing the reinforcement of the infill wall

- After deleting the reinforcement in the wall, the analysis was performed and the load – deflection curve came exactly as that incase of the original reinforcement. The stresses in the wall have been subject to a negligible increased. (Fig. 4.1)
- After doubling the reinforcement, the analysis was performed where the load – deflection curve came exactly as that incase of the original reinforcement. The stresses in the steel grid have been subject to a negligible decreased. (Fig. 4.1)

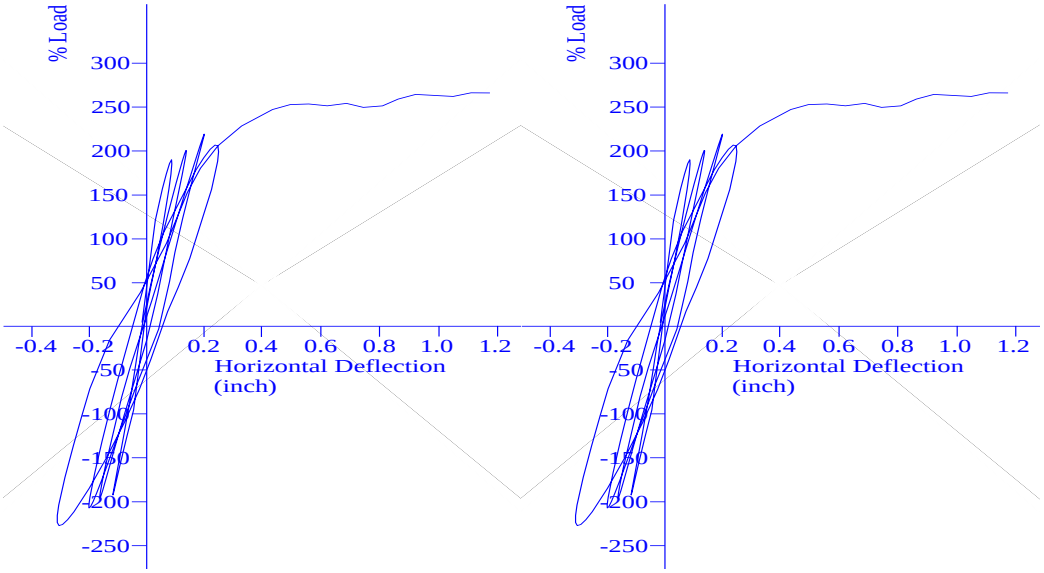

Figure 4.1 The Load – Deflection curve for the model incase of having a P.C. infill wall (left) and that with the reinforcement in the infill wall doubled (right).

N.B. For more details please refer to section 4.3.

4.2 Changing the thickness of the infill wall

The thickness of the infill wall (with the filled gap) has been changed, and the analysis was performed for each thickness (b). A summary of the results is presented in Table 4.1:

Table 4.1 Summary of the parametric study on the thickness of the infill wall.

b (in)	b (mm)	F_{max}	% change in thickness	% change in force	$b/b_{original}$	$F_{max}/F_{maxoriginal}$
4	**101.6**	2.57	-33.33%	-3.75%	0.67	0.96
5	**127**	2.6	-16.67%	-2.62%	0.83	0.97
6	**152.4**	2.67	0.00%	0	1.00	1.00
8	**203.2**	2.79	33.33%	4.49%	1.33	1.04
9	**228.6**	2.82	50.00%	5.62%	1.50	1.06
10	**254**	2.87	66.67%	7.49%	1.67	1.07
12	**304.8**	2.92	100.00%	9.36%	2.00	1.09

b: the thickness of the wall in inches.

F_{max}: the maximum seismic load that can be carried by the system divided by the maximum seismic load that can be carried by the bare frame.

$F_{max\ original}$: the maximum seismic load that can be carried by the system when the thickness of the wall is equal to 6 inches divided by the maximum seismic load that can be carried by the bare frame.

$b_{original}$: the thickness of the original infill wall which is equal to 6 inches.

$F_{max}/F_{max\ original}$: the ratio between maximum seismic load that can be carried by the system and the maximum seismic load that can be carried by the system when the thickness of the wall is equal to 6 inches.

$b/b_{original}$: the ratio between the thickness of the wall and the thickness of the original infill wall.

The load – deflection curves of the several models have been plotted and are shown in Fig. 4.2. The increase in seismic strength resulting from increasing the thickness of the infill wall to double its original thickness is less than 10 % and the decrease in seismic strength resulting from decreasing the thickness of the infill wall to two thirds of its original thickness is less than 4 % as shown in Fig. 4.3.

The results mentioned previously could be validated using a finite element model on SAP. The wall was represented by a cross bracing system where each brace has a cross-section of 40 inch x 6 inch. The analysis was performed and the bending moment at the bottom of the column was 45.78 Kip.inch. When the thickness of the braces was changed to be 12 inch and the model was re-analyzed and the bending moment at the bottom of the column was 40.18 Kip.inch (see Appendix B). Therefore it could be concluded that doubling the thickness of the braces increased the maximum lateral load that could be carried by the system by 13.94 %. When comparing this increase to the 9.36% reported in table 4.1 it could be said that the analysis performed using DIANA is valid. The increase of 9.36% is more accurate than the increase of 13.94 % due to DIANA performing a non-linear analysis while SAP performed a linear analysis.

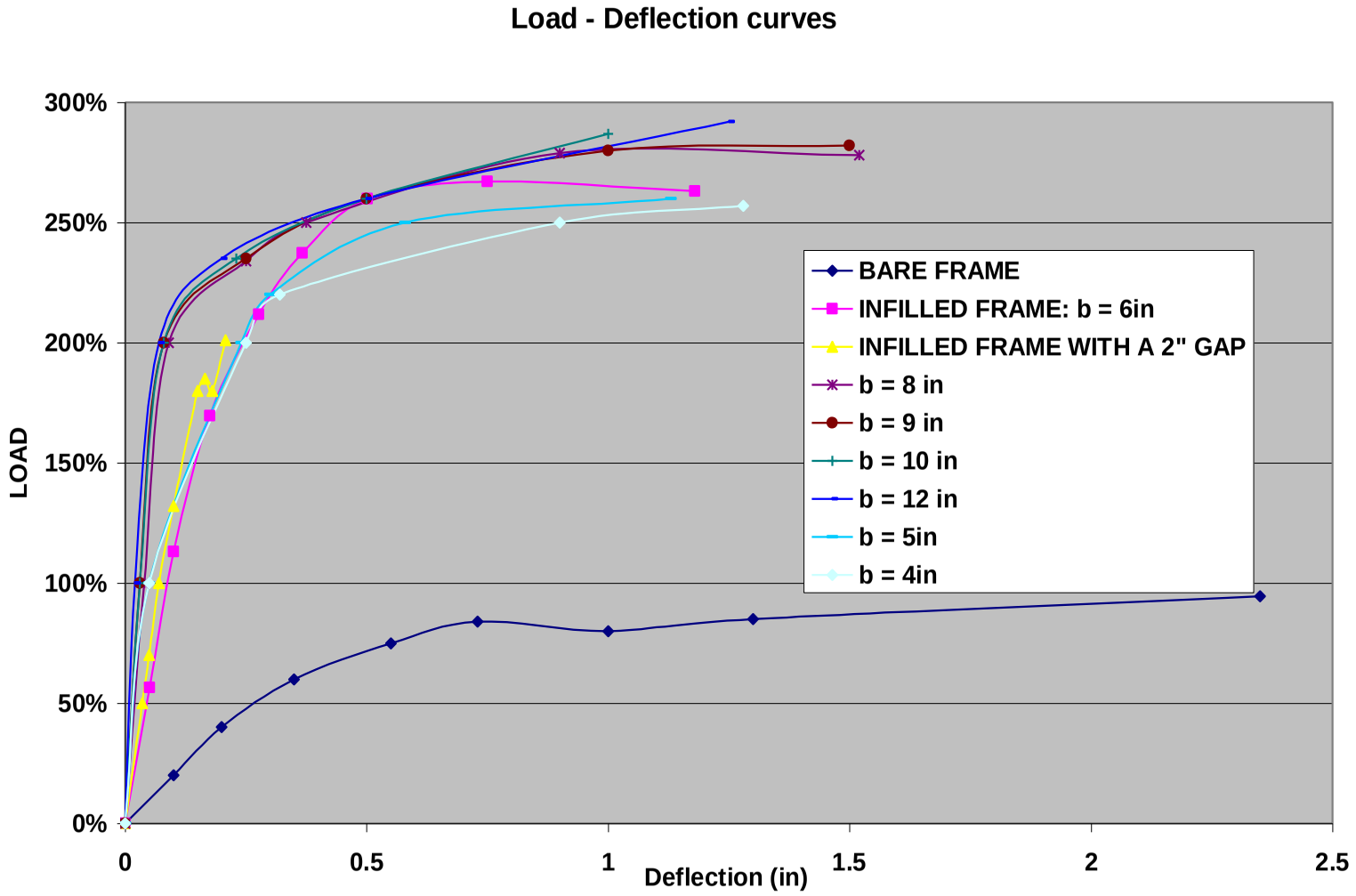

Figure 4.2 Load – Deflection curves for various values of wall thickness.

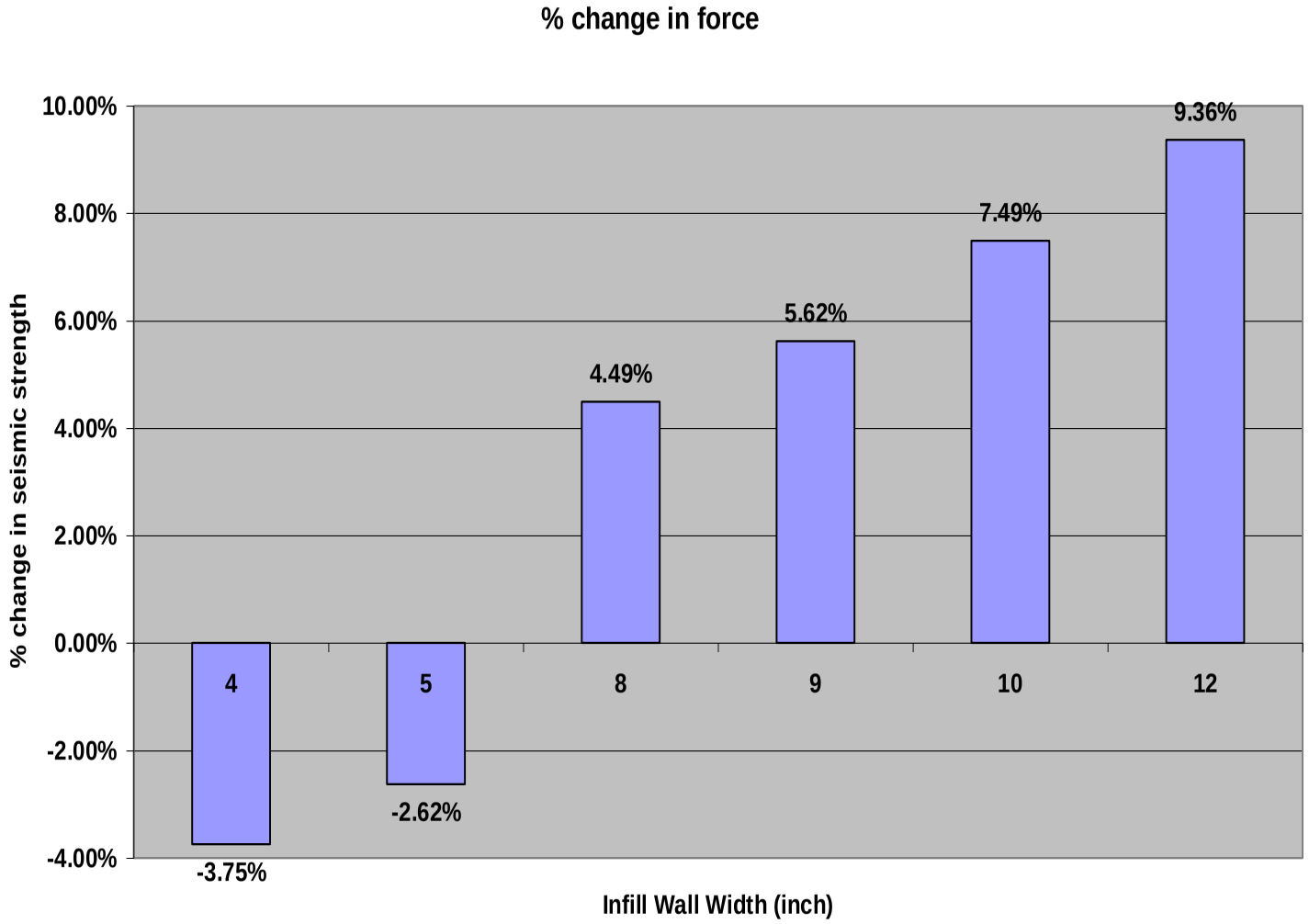

Figure 4.3The effect of changing the wall thickness on the seismic strength.

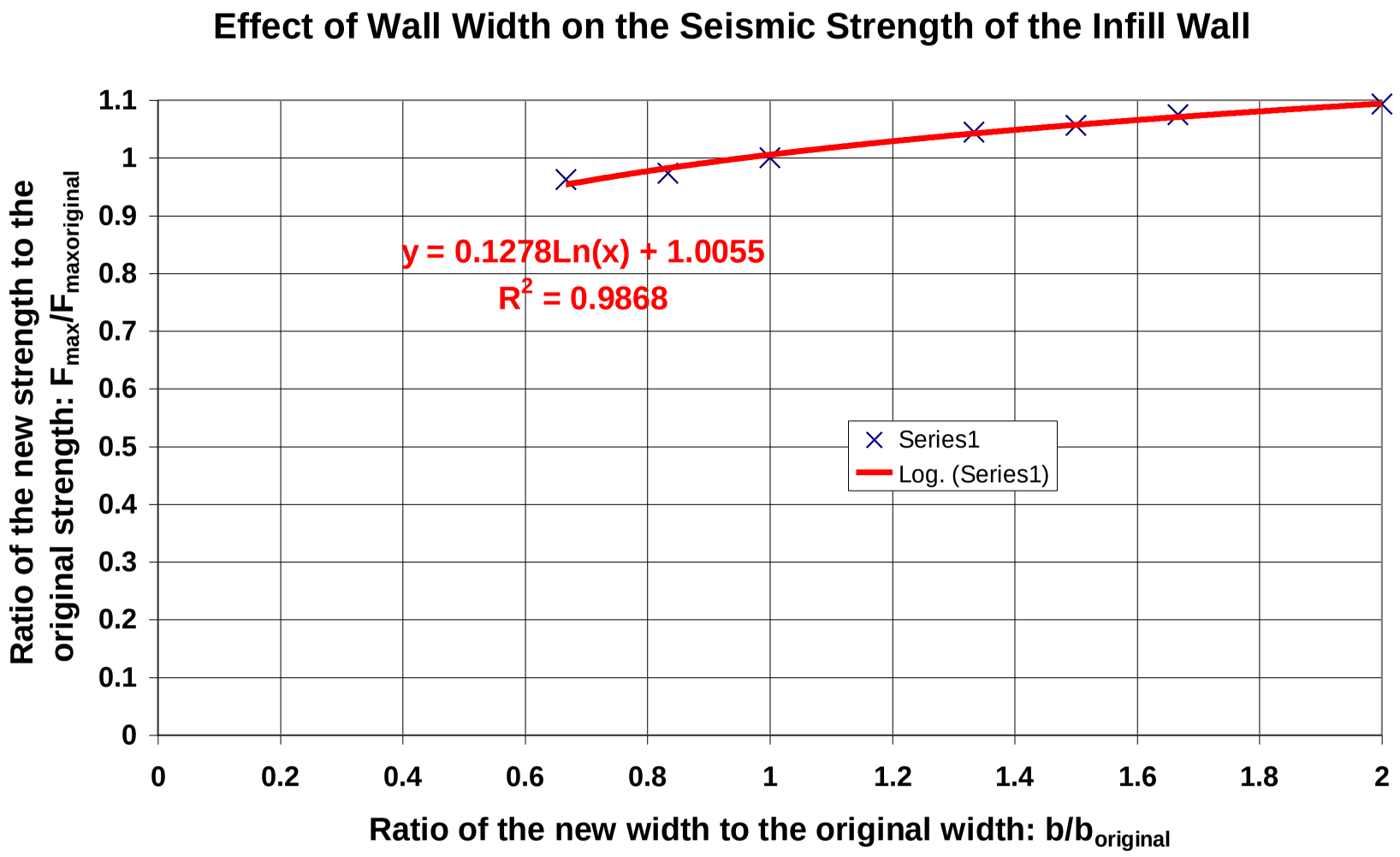

Figure 4.4 The relation between $b/b_{original}$ and $F_{max}/F_{max\ original}$.

The relation shown in figure 4.4 can be represented by the following equation:

$$F_{max}/F_{max\ original} = 0.1278\ln(b/b_{original}) + 1 \qquad (4.1)$$

The correlation coefficient (R^2) of the equation above is 0.9868 therefore the coefficient of determination (R) is 0.99337 i.e. the results produced by the above equation are 99.337 % accurate.

4.3 Changing the reinforcement of the columns

Although it is not possible in the real problem to change the reinforcement of the columns as this is a retrofit technique. It was interesting to investigate the effect of that parameter on the performance of the infilled frame system keeping the length of the lap splice unchanged.

The reinforcement in the columns was increased by 20 % and then decreased by 20 % so as to see the effect of the change in the quantity of steel inside the columns on the shape and size of the cracks inside the infill wall. The results are shown in Fig. 4.5 and 4.6.

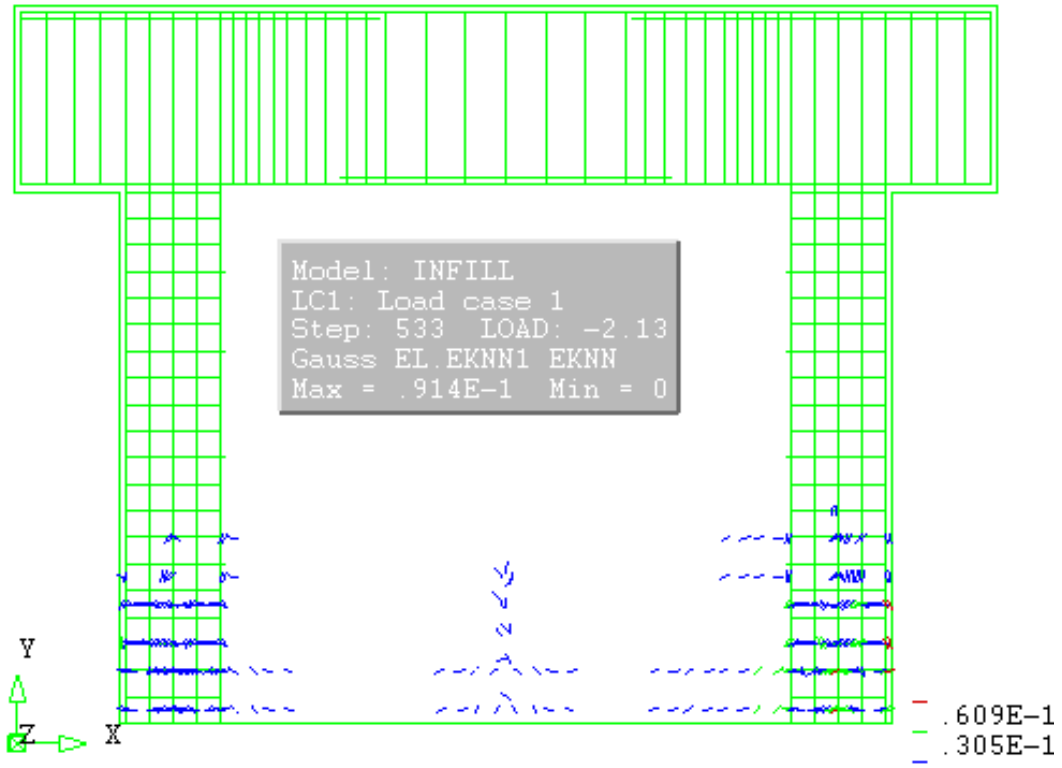

Figure 4.5 Cracking pattern of the infilled frame with a 20 % reduction in the Column reinforcement.

The size of the cracks remained the same but the frequency of the cracks changed. On increasing the steel the number of cracks in the two lower corners of the wall increased together with the number of cracks in the middle but no bridging has occurred between the cracks. Decreasing the column reinforcement by 20 % decreased the maximum seismic load to 142.28 Kips (632.89 KN) which is equivalent to 80 % of the maximum seismic load before this reduction. Increasing the column reinforcement by 20 % increased the maximum seismic load to 181.03 Kips (805.26 KN) which is equivalent to 101.7 % of the maximum seismic load before this increase.

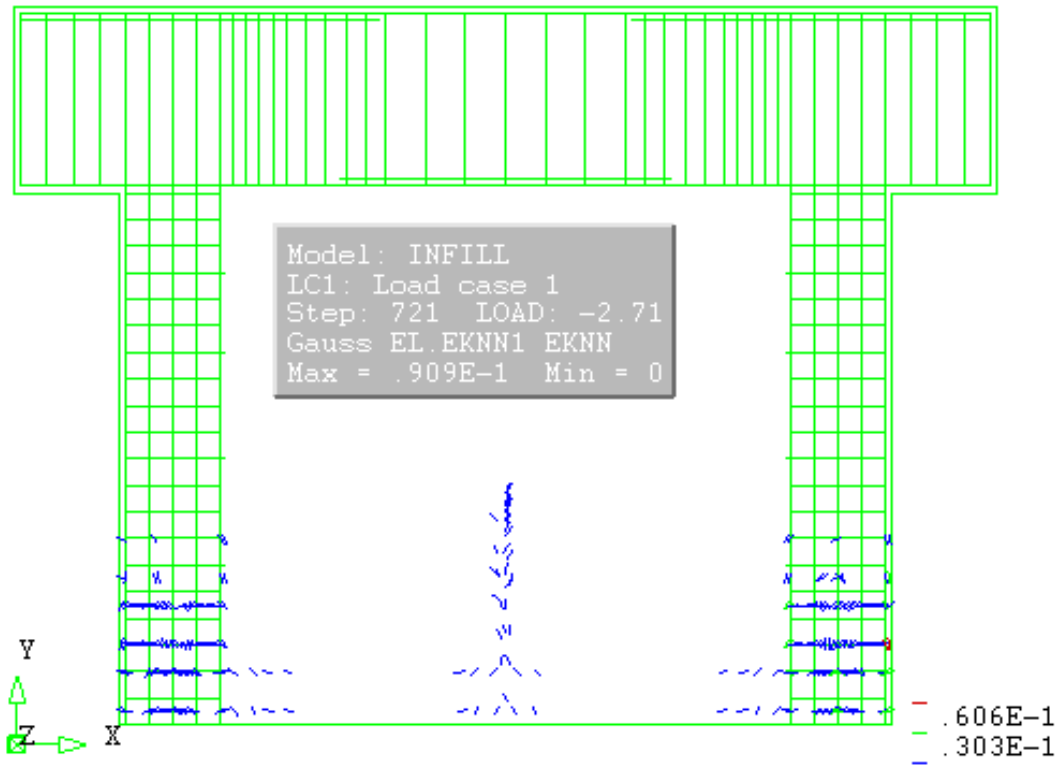

Figure 4.6 Cracking pattern of the infilled frame with a 20 % increase in the Column reinforcement.

These results support the results reported in section 4.1 as the major cracks occur in the columns and are significantly larger than the cracks in the wall which implies that the tensile stresses in the wall are much less than these in the columns due to seismic load. The experimental results observed by Haroun et al [3] showed neglegible cracks occurring in the wall. Therefore it is not expected to find that the steel mesh in the wall to have an effect on the seismic strengthening of the structure.

4.4 Changing the concrete strength of the infill wall

The concrete strength of the infill wall (of the filled gap) has been changed (keeping the concrete in the frame as is) then the analysis was performed for each of the concrete compressive strengths (f_{cu}), the results are presented in table 4.2:

Table 4.2 The parametric study on the concrete strength of the infill wall.

f_{cu} (psi)	f_{cu} (MPa)	F_{max}	% change in f_{cu}	% change in force	$fcu/f_{cu\ original}$	$F_{max}/F_{max\ original}$
3000	**26.89**	2.44	-40.00%	-8.61%	0.6	0.91
3500	**31.371**	2.608	-30.00%	-2.32%	0.7	0.98
4000	**35.853**	2.66	-20.00%	-0.37%	0.8	1.00
4500	**40.334**	2.66	-10.00%	-0.37%	0.9	1.00
5000	**44.816**	2.67	0.00%	0	1	1.00
5500	**49.298**	2.7	10.00%	1.12%	1.1	1.01
5750	**51.538**	2.8	15.00%	4.87%	1.15	1.05

f_{cu} : the concrete compressive strength of the wall in psi.

F_{max}: the maximum seismic load that can be carried by the system divided by the maximum seismic load that can be carried by the bare frame.

$F_{max\ original}$: the maximum seismic load that can be carried by the system when the concrete compressive strength of the wall is equal to 5000 psi divided by the maximum seismic load that can be carried by the bare frame.

$f_{cu\ original}$: the concrete strength of the original infill wall which is equal to 5000 psi.

$F_{max}/F_{max\ original}$: the ratio between maximum seismic load that can be carried by the system and the maximum seismic load that can be carried by the system when the concrete compressive strength of the wall is equal to 5000 psi.

$f_{cu}/f_{cu\ original}$: the ratio between the concrete compressive strength of the wall and the concrete compressive strength of the original infill wall.

$\Delta F_{max}/F_{max\ original}$: the relative change in the seismic strength.

$\Delta f_{cu}/f_{cu\ original}$: the relative change in the concrete compressive strength of the wall.

N.B.The values in MPa have been factored so as to convert them from a cylinder system to a cube system).

The increase in seismic strength resulting from increasing the concrete strength by 15 % is less than 5 % and the decrease in seismic strength resulting from decreasing the concrete strength of the infill wall to 60 % of its original concrete strength is less than 9 % as shown in Fig. 4.7.

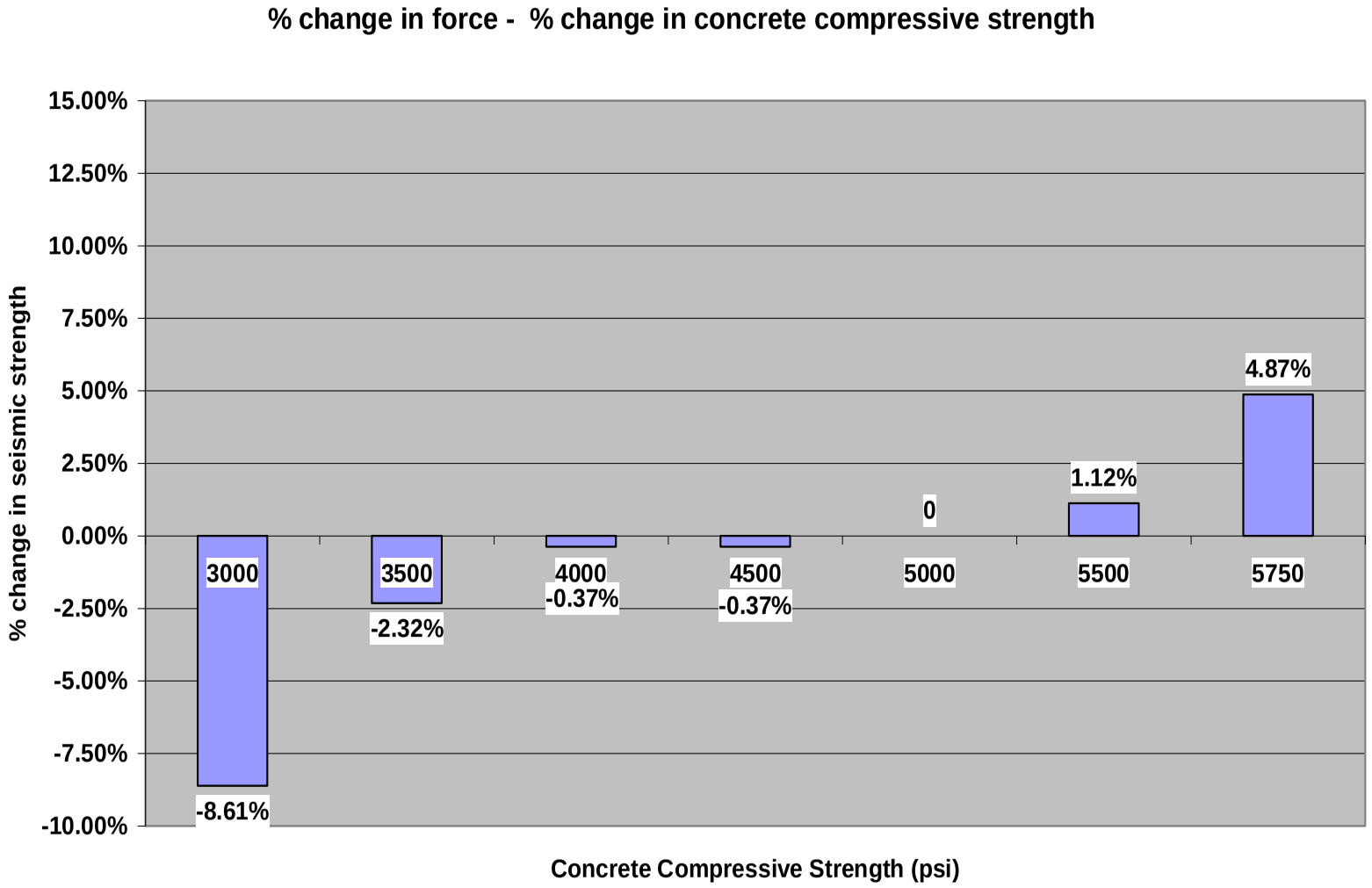

Figure 4.7 The effect of changing the wall concrete strength on the seismic strength

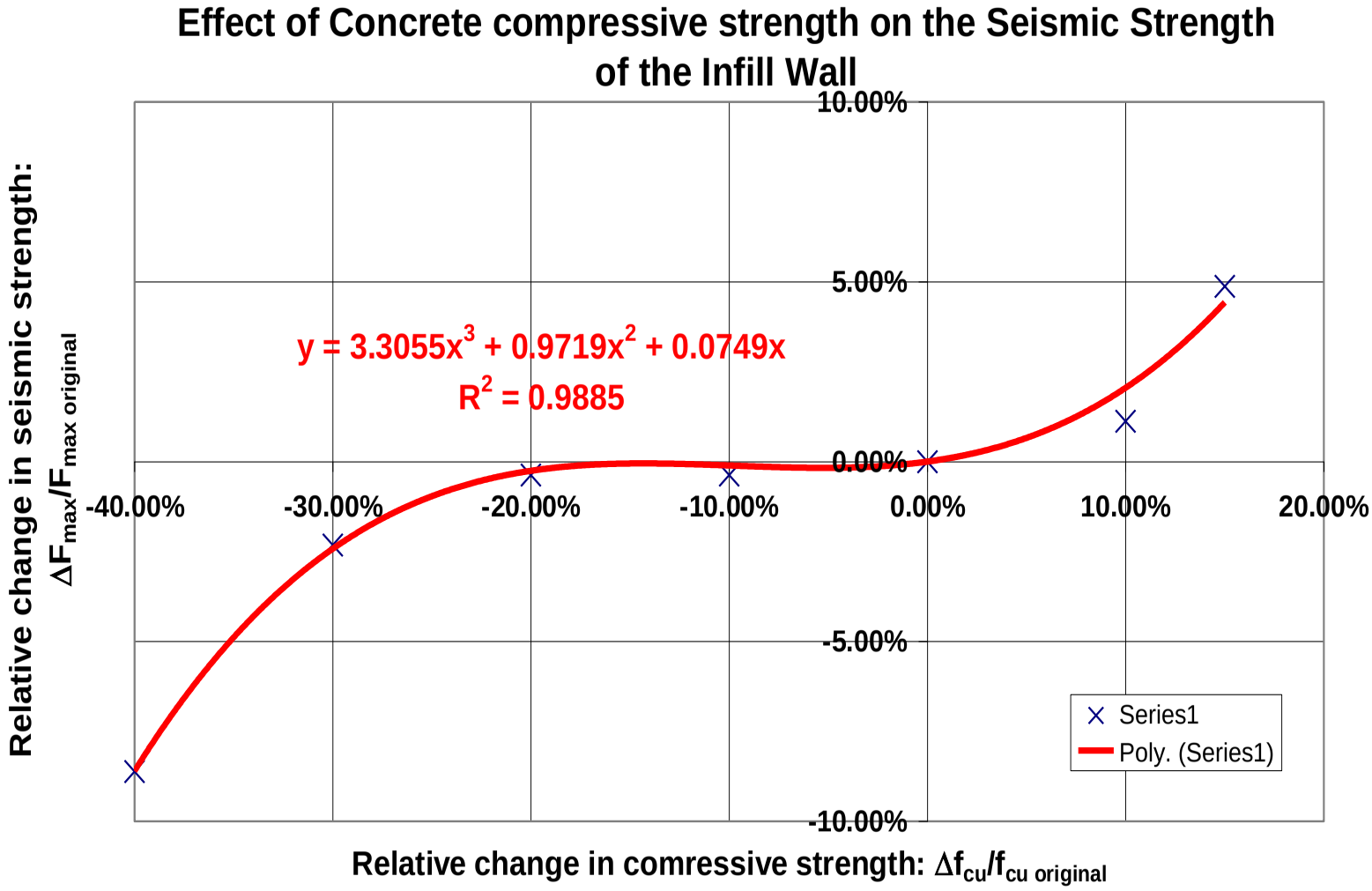

Figure 4. 8 The relation between the relative change in the wall concrete strength and the relative

The relation shown in Fig. 4.8 can be represented by the following equation:

$$\Delta F_{max} / F_{max\ original} =$$
$$3.31(\Delta f_{cu}/f_{cu\ original})^3 + 0.97(\Delta f_{cu}/f_{cu\ original})^2 + 0.075\Delta f_{cu}/f_{cu\ original} \qquad (4.2)$$

The correlation coefficient (R^2) of the equation above is 0.9885 therefore the coefficient of determination (R) is 0.9943 i.e. the results produced by the above equation are 99.43 % accurate.

CHAPTER5: CONCLUSIONS AND RECOMMENDATIONS

5.1 Conclusions

5.1.1 Validation and calibration of the finite element model

The model is valid and has been successfully calibrated. The numerical model of sample # 4 – which was the model used later to perform the parametric study – was highly accurate in representing the maximum lateral strength and 87.6 % accurate in representing the maximum lateral deflection.

5.1.2 Effect of the reinforcement of the infill wall

Based on the results reported in the experimental work conducted by Haroun et al and the results reported in sections 4.1 and 4.3 there is no evidence that the reinforcement of the infill wall had an effect on the seismic strength of the system or on its ductility.

5.1.3 Effect of the thickness of the infill wall

- The increase in seismic strength resulting from increasing the thickness of the infill wall to double its original thickness is less than 10 %.
- The decrease in seismic strength resulting from decreasing the thickness of the infill wall to two thirds of its original thickness is less than 4 %.
- The effect of the thickness on the seismic strength of the system can be represented by the following equation (section 4.2):

$$F_{max} / F_{max\ original} = 0.1278 \ln(b / b_{original}) + 1 \qquad (4.1)$$

5.1.4 Effect of the reinforcement of the columns

- The reinforcement of the columns had a direct effect on the seismic strength of the system as when the reinforcement of the columns is reduced the seismic strength of the system decreases while when the reinforcement of the columns is increased the seismic strength of the system increases.

- Based on the results reported in the experimental work conducted by Haroun et al and the results reported in section 4.3 the reinforcement of the columns had a small effect on the cracking pattern in the infill wall which is expected as the major cracking occurs in the columns.

5.1.5 Effect of the concrete strength of the infill wall

- The increase in seismic strength resulting from increasing the concrete compressive strength of the infill wall by 15 % of its original concrete compressive strength is less than 5 %.
- The decrease in seismic strength resulting from decreasing the concrete compressive strength of the infill wall to 60 % of its original concrete compressive strength is less than 9 %.
- The effect of the width on the seismic strength of the system can be represented by the following equation (section 4.4):

$$\Delta F_{max} / F_{max\ original} = 3.31(\Delta f_{cu}/f_{cu\ original})^3 + 0.97(\Delta f_{cu}/f_{cu\ original})^2 + 0.075\Delta f_{cu}/f_{cu\ original} \quad (4.2)$$

5.2 Recommendations

5.2.1 Recommendations when using the infill wall method

- Using reinforced concrete infill walls with a minimum reinforcement is more economic than using a dense mesh and produce the same effect.
- The standard wall thickness of all infill walls adopted by caltrans is 18 inch (0.45 m). However it has been proven that decreasing it to 12 inch (0.305 m) will only reduce the seismic strength by 3.75 %.
- It has been proven that decreasing the compressive strength of the infill wall from 5000 psi – which is the commonly used in U.S. bridges – to 3000 psi will only reduce the seismic strength by 8.61 %. Hence in some countries it would be more economic to reduce the concrete strength without having a large sacrifice of seismic strength.

5.2.2 Recommendations for future research

- Studying the effect of the length and position of the lap splice in the columns on the seismic strength of the infill wall system.
- Performing an economic analysis so as to compare the different methods of seismic strengthening.
- Studying the combined effect of changing the thickness, concrete strength and reinforcement together on the seismic strength of the infill wall system.

References

[1]. Penelis, G.G. and Kappos, A.J. "*Earthquake Resistant Concrete Structures*" E & FN Son, 1997.

[2]. Chen, Wai Fah and Scawthorn, Charles. "*Earthquake Engineering Handbook*" CRC Press, Inc., 2003.

[3]. Haroun, M.A. and Elbahar, M.R. "*Testing of Column Bents Strengthened by Infill Walls*" Final Report to the California Department of Transportation, Department of Civil and Environmental Engineering, University of California, Irvine, June 2002.

[4]. ACI341.2R-97, "*Seismic Analysis and Design of Concrete Bridge Systems"* American Concrete Institute, Report No. 341.2R-97, 1997.

[5]. Saiidi, Mehdi "*Current Bridge Seismic Retrofit Practice in the United States*" Seismic Design and Construction. American Concrete Institutes Compilation 31, 1992.

[6]. Yu, Lei; Yao, Qian-Feng; Yue, Ya-Feng. Analysis of stiffness and load-resisting capacity of fundamental frame structures in high-performance concrete multi-rib walls. Science Press, Beijing, China: v 38 p 23-29 February 2006.

[7]. Al-Muyeed, Abdullah; Afrin, Rumana. Effect of masonry infill for reducing the sway of RC frame using finite element modeling. Journal of Construction Research: v 6 p 293-306 September 2005.

[8]. Yeh, Yung-Hsin; Liao, Wen-I. Cyclic performance of two-story ductile RC frames with infill walls. ASME Pressure Vessels Piping Div. Publ. PVP: v 8 p 259-264 July 2005.

[9]. Perera, Ricardo. Performance evaluation of masonry-infilled RC frames under cyclic loading based on damage mechanics. Engineering Structures: v 27 p 1278-1288 July 2005.

[10]. DIANA online documentation; March 2006.